

Quantum phase transition of Ising-coupled Kondo impurities

M. Garst^a, S. Kehrein^b, T. Pruschke^b, A. Rosch^a, and M. Vojta^a

^a*Institut für Theorie der Kondensierten Materie,*

Universität Karlsruhe, Postfach 6980, 76128 Karlsruhe, Germany

^b*Theoretische Physik III, Elektronische Korrelationen und Magnetismus,*

Universität Augsburg, 86135 Augsburg, Germany

(Dated: February 10, 2004)

We investigate a model of two Kondo impurities coupled via an Ising interaction. Exploiting the mapping to a generalized single-impurity Anderson model, we establish that the model has a singlet and a (pseudospin) doublet phase separated by a Kosterlitz-Thouless quantum phase transition. Based on a strong-coupling analysis and renormalization group arguments, we show that at this transition the conductance G through the system either displays a zero-bias anomaly, $G \sim |V|^{-2(\sqrt{2}-1)}$, or takes a universal value, $G = \frac{e^2}{\pi h} \cos^2\left(\frac{\pi}{2\sqrt{2}}\right)$, depending on the experimental setup. Close to the Toulouse point of the individual Kondo impurities, the strong-coupling analysis allows to obtain the location of the phase boundary analytically. For general model parameters, we determine the phase diagram and investigate the thermodynamics using numerical renormalization group calculations. In the singlet phase close to the quantum phase transition, the entropy is quenched in two steps: first the two Ising-coupled spins form a magnetic mini-domain which is, in a second step, screened by a Kondo-like collective resonance in an effective *solitonic* Fermi sea. In addition, we present a flow equation analysis which provides a different mapping of the two-impurity model to a generalized single-impurity Anderson model in terms of fully renormalized couplings, which is applicable for the whole range of model parameters.

I. INTRODUCTION

Kondo physics plays a fundamental role for the low-temperature behavior of a large variety of physical systems like magnetic impurities in metals, heavy fermion systems, glasses, quantum dots, etc. Its key feature is the quenching of the impurity entropy through non-perturbative screening by many-particle excitations in the associated quantum bath. For magnetic impurities in metals this amounts to the formation of the Kondo singlet between the localized spin and electron-hole excitations in the Fermi sea.¹

Most of the aspects of single-impurity Kondo physics are now well understood after theoretical tools have been developed that can deal with its intrinsic strong-coupling nature.^{1,2,3} However, in many physical systems the interaction of different impurities, i.e., multi-impurity Kondo physics, is important. For example in heavy fermion systems the RKKY interaction between different impurity spins leads to competition between local Kondo physics and long-range magnetic order that determines their phase diagram.⁴ More recently, related questions about coupled two-level systems have gained much interest in quantum computation, where decoherence due to unwanted couplings among qubits and between qubits and environment should be avoided; on the other hand the intentional coupling of qubits is the key step to performing quantum logic operations.

In the present paper we investigate the case of two spin-1/2 Kondo impurities $\mathbf{S}_1, \mathbf{S}_2$ coupled via a Ising coupling,

$$H_{12}^{\text{Ising}} = K_z S_1^z S_2^z. \quad (1)$$

The Kondo coupling of each impurity to its bath is given

by

$$H_j^K = 2J_{\perp}(S_j^x s_{0,j}^x + S_j^y s_{0,j}^y) + 2J_z S_j^z s_{0,j}^z \quad (2)$$

where $j = 1, 2$ labels the impurity, and $\mathbf{s}_{0,j}$ is the bath spin operator at the respective impurity site. Furthermore the two baths are disconnected.

Two impurities coupled both to baths and among each other present the simplest realization of the so-called cluster Kondo effect, which has been discussed, e.g., in context of disordered Kondo-lattice compounds.⁵ Furthermore, the dynamics of magnetic droplets or domains, formed in disordered itinerant systems near a magnetic quantum phase transition,⁶ also leads to models of coupled impurities like the one considered here. Therefore, we will also refer to the two coupled impurities as magnetic “mini-domain”.

In the context of Kondo impurities, an Ising-like coupling (1) can be thought of as an effective impurity interaction for heavy fermion systems with an easy axis. Also, Ising coupling appears naturally in quantum dots that are coupled via their mutual capacitance⁷ here the two-level systems are pseudospins representing the number of electrons on the dots, and therefore SU(2) symmetry is broken from the outset.^{8,9,10} Equivalently, one can think of two two-level systems with transversal coupling, with the experimental realization of coupled flux qubits.¹¹ We will discuss different formulations and applications of our model in the body of the paper.

Coupled impurities or two-level systems have been investigated in a number of papers,^{12,13,14,15,16,17,18,19} where most attention has been focussed on the case of SU(2)-symmetric direct exchange coupling between the impurity spins, $K \mathbf{S}_1 \cdot \mathbf{S}_2$. Here, two different regimes are possible as function of the inter-impurity exchange K :

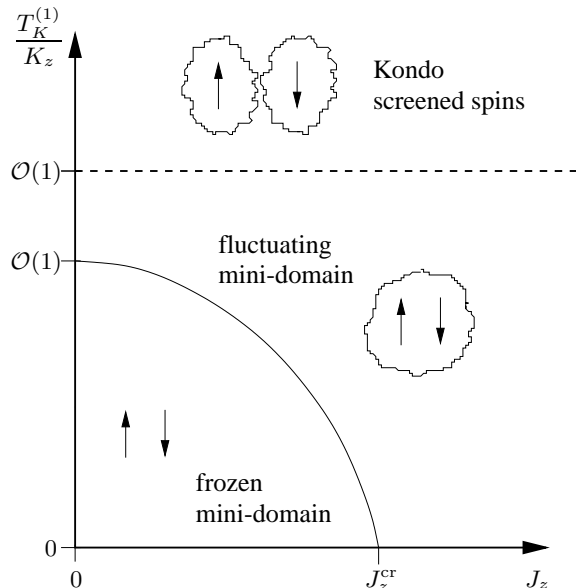


FIG. 1: Schematic phase diagram for two Ising-coupled Kondo impurities (1,2). The vertical axis denotes the ratio between single-impurity Kondo temperature $T_K^{(1)}$ (determined by the Kondo couplings J_z , J_\perp , and the bath bandwidth D) and Ising coupling K_z . The horizontal axis (J_z) measures the anisotropy of the Kondo coupling; in the universal regime, $T_K^{(1)} \ll D$, isotropic Kondo coupling corresponds to $J_z \ll J_z^{cr}$. The model has two phases: At small J_z and large K_z , the ground state is doubly degenerate and the two impurity spins are locked into a “frozen mini-domain”. In contrast, at large J_z or small K_z the ground state is a singlet with local Fermi-liquid characteristics. The quantum phase transition is of Kosterlitz–Thouless type. In the universal regime, $T_K^{(1)} \ll D$ implying $J_\perp \ll D$, $T_K^{(1)}$ is the only low-energy scale of the single-impurity problem, and the phase transition occurs at a critical K_z proportional to $T_K^{(1)}$ with the proportionality factor depending on J_z , as shown in the figure (solid line). The critical K_z diverges as $J_z \rightarrow J_z^{cr}$. Below the dashed crossover line the two spins form an Ising mini-domain: the low-energy fluctuations are associated with the pseudospin degree of freedom, i.e., for antiferromagnetic K_z the staggered impurity susceptibility is much larger than the uniform one.

for large antiferromagnetic K the impurities combine to a singlet, and the interaction with the conduction band is weak, whereas for ferromagnetic K the impurity spins add up and are Kondo-screened by conduction electrons in the low-temperature limit. Notably, there is *no* quantum phase transition as K is varied in the generic situation without particle–hole symmetry (whereas one finds an unstable non-Fermi liquid fixed point in the particle–hole symmetric case).^{13,14,16}

As has been pointed out by Andrei *et al.*,²⁰ the case of Ising coupling is different and particularly interesting, because for large $|K_z|$ the two Ising-coupled spins form a magnetic mini-domain which still contains an internal degree of freedom as the ground state of H_{12}^{Ising} is doubly degenerate (in contrast to the inter-impurity singlet mentioned above). For the case of antiferromagnetic K_z

(which we will assume in the following), the two low-energy states of the impurities (forming a pseudospin) are $|\uparrow\downarrow\rangle$ and $|\downarrow\uparrow\rangle$. As we will show in this paper, the fate of this pseudospin degree of freedom depends on the strength and asymmetry of the Kondo coupling J between the spins and the bath electrons.

A. Summary of results

Here, we will summarize our main results which are detailed in the body of the paper, and schematically represented in the phase diagram of Fig. 1. A brief summary of the methods used to obtain these results is given below in Sec. IB.

The model of two Ising-coupled impurities, connected to two *separate* fermionic reservoirs (realized, e.g., by attaching two separate leads to two quantum dots, Fig. 2), has two ground-state phases associated to either a screened or an unscreened pseudospin. For small Kondo couplings J_\perp , J_z and large K_z , tunneling between the two pseudospin configurations, $|\uparrow\downarrow\rangle$ and $|\downarrow\uparrow\rangle$, is suppressed at low energies, i.e., the mini-domain is “frozen” as $T \rightarrow 0$, and the ground state entropy is $S_0 = \ln 2$. In contrast, for small K_z the two impurities are individually Kondo screened, resulting in a Fermi-liquid phase with vanishing residual entropy. This implies the existence of a quantum phase transition for $K_z \sim T_K^{(1)}$, where $T_K^{(1)}$ is the single-impurity Kondo temperature. For isotropic Kondo coupling, i.e., small J_z , this has been previously pointed out by Andrei *et al.*²⁰

What is the nature of this phase transition? Does it occur by breaking up the Ising-coupled mini-domain, or rather by strong fluctuations of the preformed pseudospin? What are the universal properties of this transition? The key observation, which helps to answer these questions, is that the system can also be tuned towards the quantum phase transition by increasing the Ising component, J_z , of the coupling of the spins to the environment in a regime where $K_z \gg T_K^{(1)}$ (see Fig. 1). For $K_z \gg T_K^{(1)}$ the mini-domain is stable. However, upon increasing J_z a many-particle effect (related to formation of a Mahan exciton²¹) enhances the tunneling between the two configurations, $|\uparrow\downarrow\rangle$ and $|\downarrow\uparrow\rangle$, of the mini-domain. If J_z exceeds a critical value, J_z^{cr} , this tunneling can quench the pseudospin even for infinitesimal $T_K^{(1)}$ (equivalent to infinitesimal transverse Kondo coupling J_\perp).

The resulting phase of the “fluctuating mini-domain” is actually a Fermi liquid with vanishing residual entropy. Note that the finite-temperature properties in this regime are rather different from that of the Fermi liquid which is obtained for $T_K^{(1)} \gg K_z$. For large J_z and small J_\perp , the high-temperature $\ln 4$ impurity entropy is quenched in two stages: first, at the scale $T^0 \approx K_z$, the mini-domain “forms”, quenching half of entropy; second the strong fluctuations kill the remaining $\ln 2$ entropy at a much lower scale T^* , this scale T^* can be identi-

fied with a collective Kondo temperature associated to pseudospin screening. (Note that this type of two-stage screening is completely different from the one occurring for two conventional Kondo screening channels with different strengths.¹²) In contrast, for $T_K^{(1)} \gg K_z$ the entropy of the two spins is quenched simultaneously in a single step at the scale $T_K^{(1)}$. Nevertheless, the two Fermi-liquid regimes are adiabatically connected by a smooth crossover, which we will show to be identical to the well-known crossover in the single-impurity Anderson model from the mixed valence into the Kondo regime.

The quantum phase transition at $J_z = J_z^{cr}$ turns out to be in the Kosterlitz–Thouless universality class. Assuming continuity along the phase boundary (which we verified numerically), this is true for the transition at arbitrary $J_z \leq J_z^{cr}$. Furthermore, universality immediately implies that the “fluctuating mini-domain” regime with its characteristic two-stage quenching of the entropy also exists for small J_z close to the quantum phase transition (see Fig. 1).

Physical observables, like the conductance in a quantum dot setup, show *universal* behavior in the vicinity of the phase boundary. Therefore, we can calculate them close to J_z^{cr} (see Fig. 1), where the phase transition takes place in a regime of large K_z being accessible to a strong-coupling analysis combined with renormalization group arguments. Depending on the experimental setup, we find, e.g., a conductance anomaly characterized by the exponent $-2(\sqrt{2}-1)$, or a universal conductance $e^2 \cos^2 \left[\frac{\pi}{2\sqrt{2}} \right] / (\hbar\pi)$ at the phase transition. We emphasize again that these results are valid close to the quantum phase transition even for small J_z where a strong-coupling analysis is not possible.

B. Methods and outline

To obtain the physical picture and the results described above, we use a combination of six different and partly complementary methods.

In Sec. II we (i) map our model of Ising-coupled spins to a generalized Anderson model by bosonization and refermionization techniques. This mapping is used to obtain the qualitative structure of the phase diagram and analytic results for the phase boundary at large J_z . Furthermore, for the generalized Anderson model it is much easier to implement (ii) numerical renormalization group (NRG), which is presented in Sec. IV. With the help of NRG it is possible to determine numerically the phase boundaries in regimes not accessible to analytic methods. Furthermore, NRG is essential to establish that the phase transition at small J_z is continuously connected to the one at large J_z .

Making use of this adiabatic continuity is the main idea of this paper to obtain analytic results for the quantum phase transition. By increasing J_z we can tune the transition from a regime with $K_z \sim T_K^{(1)}$ to a regime

with $K_z \gg T_K^{(1)}$, where we can employ (iii) a strong-coupling expansion (Sec. III). The strong-coupling result is analyzed using (iv) perturbative renormalization group, or more precisely power counting, taking into account the anomalous dimensions created from an orthogonality catastrophe. Using these methods the phase diagram for large $K_z \gg T_K^{(1)}$ and the precise position of the critical point for $K_z \rightarrow \infty$ can be obtained. In addition, we can determine the relevant phase shifts and scaling dimensions of leading relevant and irrelevant operators (Sec. VI). This allows us to analytically calculate the conductance and zero-bias anomalies close to the quantum phase transition for *arbitrary* values of $T_K^{(1)}/K_z$, see Sec. VII. To analytically obtain the precise shape of the phase diagram for large J_z , we develop in App. A (v) a generalization of the Schrieffer–Wolff transformation to take into account the short-range density interaction of our generalized Anderson model, leading to associated power-law singularities.

In Sec. V and App. B we re-derive some above results independently by using (vi) flow equations. The advantage of this method is that it has a broad range of applicability and gives a more natural description in terms of renormalized quantities. The flow equation mapping nicely establishes the equivalence of the different Fermi-liquid regimes of the model. It also allows us to derive the full phase diagram analytically for general values of the coupling J_z that are not accessible with the strong-coupling expansion.

Transport quantities and corresponding possible experimental realizations are discussed in Sec. VII. The most promising way to implement Ising-coupled (pseudo)spin variables is the use of charge degrees of freedom of two quantum dots, following Matveev’s proposal^{8,9}, and employ a capacitive coupling which takes the role of K_z , see Sec. VII A.

Most of our methods are based on the mapping of the original two-impurity model to a generalized single-impurity Anderson model, except for the strong-coupling analysis in Sec. III A which is applied to the original model (and thus directly establishes the existence of a phase transition). As we will show, the employed mapping provides a particularly clear picture of the underlying physics, e.g., it establishes the universality class of the transition, and allows to make further progress using flow equations. Thus, the mapping turns out to be extremely helpful for obtaining the complete picture presented below.

II. MODEL: VARIATIONS AND TRANSFORMATIONS

In this section we discuss the various formulations of the model under consideration, together with the mapping between them, which is based on the well-known relation between the spin-boson model and the anisotropic Kondo model.^{3,22,23}

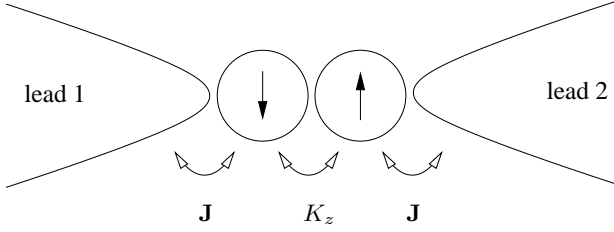


FIG. 2: Schematic plot of a system represented by the Hamiltonian (3). Two spins are coupled via an (anisotropic) exchange interaction J to two leads. The spins interact via an Ising coupling K_z . For an explicit discussion of possible experimental setups see Sec. VII.

Throughout this paper, we will consider the so-called scaling limit where both K_z and the single-impurity Kondo temperature $T_K^{(1)}$ are much smaller than the high-energy cutoff D of the theory, $T_K^{(1)}, K_z \ll D$. Keeping $J_z \geq 0$ and D fixed, this implies $J_\perp \rightarrow 0$. Only in this scaling limit the models discussed below can be mapped upon each other. In general, the position of the phase boundary, i.e., the value of the critical coupling K_z^{cr} depends on microscopic details. In the scaling limit, however, $K_z^{cr}/T_K^{(1)}$ depends only on J_z which parametrizes the renormalization flow in the single-impurity model, see Sec. IV C. This universality is represented in the phase diagram in Fig. 1.

A. Ising-coupled Kondo impurities

We consider the model

$$H^K = H_1^K + H_2^K + H_{12}^{\text{Ising}}, \quad (3)$$

where two spins \mathbf{S}_1 and \mathbf{S}_2 interact by the Ising interaction (1), H_{12}^{Ising} . Each of the spins couples to a separate fermionic bath, $c_{k\alpha j}$, via an anisotropic Kondo Hamiltonian H_j^K ($j = 1, 2$), see Fig. 2,

$$H_j^K = H_0[\Psi_{\alpha,j}] + \sum_{n\alpha\beta} J_n S_j^n \Psi_{\alpha j}^\dagger(0) \sigma_{\alpha\beta}^n \Psi_{\beta j}(0) \quad (4)$$

where α, β are spin indices and $H_0[\Psi_{\alpha,j}] = \sum_{k,\alpha} \epsilon_k c_{k\alpha j}^\dagger c_{k\alpha j}$ with $\Psi_{\sigma j}(x) = \sum_k e^{-ikx} c_{k\sigma j}$. The exchange coupling is assumed to be the same for both impurities and has an anisotropic form, $J_n = (J_\perp, J_\perp, J_z)$.

The fermionic baths are assumed to be particle-hole symmetric with a bandwidth D ; for a rectangular band the density of states at the Fermi level is then $\rho_F = 1/D$. Our conclusions are not modified by the presence of a particle-hole asymmetry. A comprehensive discussion of possible modifications of our Hamiltonian (3), e.g., due to tunneling between the fermionic baths, and how they influence our results, will be given in Sec. VI.

A model of form (3) may be approximately realized with real spins in the presence of a strong Ising

anisotropy. In addition, it occurs naturally as a model for capacitively coupled quantum dots,^{8,9,10,20} where the local operators S_1^z and S_2^z describe charge states, i.e., pseudospin degrees of freedom, on the two dots. Concrete application of our results to such a situation will be discussed in Sec. VII.

B. Coupled Qubits in ohmic baths

An alternative starting point for our model of Ising-coupled impurities can be formulated in terms of two two-level systems (spin-boson models), $H^{\text{SB}} = H_1^{\text{SB}} + H_2^{\text{SB}} + H_{12}^{\text{trans}}$ with

$$H_j^{\text{SB}} = H_0[b_{kj}] + \frac{\Delta}{2} \sigma_j^x + \frac{1}{2} \sum_{k>0} \lambda_k \sigma_j^z (b_{kj} + b_{kj}^\dagger), \quad (5)$$

where $H_0[b_{kj}] = \sum_{k>0} \omega_k b_{kj}^\dagger b_{kj}$, and a transversal coupling between them,

$$H_{12}^{\text{trans}} = \frac{K_z}{4} \sigma_1^z \sigma_2^z. \quad (6)$$

Here b_{kj}^\dagger are the bosonic creation operators for heat bath $\#j$. Δ is the bare tunneling matrix element between the two levels. The impurity properties are completely parametrized by the spectral function $J(\omega) \equiv \sum_k \lambda_k^2 \delta(\omega - \omega_k)$, which we assume to be of Ohmic form, $J(\omega) = 2\alpha\omega e^{-\omega/2\omega_c}$.

One realization of this model is the interaction of tunneling centers in glasses through higher-order phonon exchange.²⁴ In the context of quantum computation this model arises in studies of decoherence of coupled superconducting qubits: the transversal coupling K_z is generated through a superconducting flux transporter, and the heat baths describe the environment leading to decoherence.^{11,25} Here, the assumption of two different baths for the two qubits is justified, e.g., if the baths model electromagnetic noise coming from read-out circuits, which are separate for each qubit.

C. Bosonization

The equivalence of H^K and H^{SB} can be explicitly shown in the framework of bosonization. Furthermore, we will demonstrate that both Hamiltonians can be mapped to a generalized Anderson impurity model. We will use this mapping extensively, both to solve the models numerically within NRG and to identify the position and nature of the quantum phase transition in certain limits analytically.

It is well known²² that both the Kondo model and the spin-boson model are equivalent to a generalized resonant-level model to be defined below. Our model, H^K and H^{SB} , however, consists of two coupled Kondo- and spin-boson Hamiltonians. The crucial point is that

the assumed coupling H_{12}^{Ising} and H_{12}^{trans} , respectively, is transformed trivially by switching between these three representations.

We start from the two Kondo Hamiltonians (4) and apply the bosonization identity

$$\Psi_{\sigma j}(x) = \frac{1}{\sqrt{2\pi a}} F_{\sigma j} e^{-i\phi_{\sigma j}(x)}, \quad (7)$$

where a is a short distance cutoff, $F_{\sigma j}$ is an anticommuting Klein factor ($\{F_{\sigma j}^\dagger, F_{\sigma' j'}\} = 2\delta_{jj'}\delta_{\sigma\sigma'}$), and $\phi_{\sigma j}$ is the corresponding bosonic field with $[\phi_{\sigma j}(x), \partial_{x'}\phi_{\sigma' j'}(x')] = 2\pi i\delta(x-x')\delta_{jj'}\delta_{\sigma\sigma'}$. Transforming to bosonic charge and spin fields, $\phi_{s/c,j} = \frac{1}{\sqrt{2}}(\phi_{\uparrow j} \pm \phi_{\downarrow j})$, the bosonized version of the Kondo Hamiltonians (4) reads

$$H_j^K = H_0[\phi_{cj}] + H_0[\phi_{sj}] + \frac{J_z}{\sqrt{2}\pi} S_j^z \partial_x \phi_{sj}(0) \quad (8) \\ + \frac{J_\perp}{2\pi a} \left(e^{-i\sqrt{2}\phi_{sj}(0)} S_j^+ F_{\downarrow j}^\dagger F_{\uparrow j} + \text{h.c.} \right),$$

where $H_0[\phi] = v_F \int \frac{dx}{2\pi} \frac{1}{2} (\partial_x \phi)^2$ assuming a linear dispersion, $\epsilon_k = v_F k$. The bosonic charge field, ϕ_{cj} , decouples and is omitted in the following.

Applying a general Emery–Kivelson transformation,²³

$$U_\gamma = \exp \left(i\gamma \sum_j S_{zj} \phi_{sj}(0) \right), \quad (9)$$

parametrized by γ , the Hamiltonian H_j^K transforms into $\tilde{H}_j^K = U_\gamma H_j^K U_\gamma^\dagger$,

$$\tilde{H}_j^K = H_0[\phi_{sj}] + \left(\frac{J_z}{\sqrt{2}\pi} - \gamma v_F \right) S_j^z \partial_x \phi_{sj}(0) \quad (10) \\ + \frac{J_\perp}{2\pi a} \left(e^{-i(\sqrt{2}-\gamma)\phi_{sj}(0)} S_j^+ F_{\downarrow j}^\dagger F_{\uparrow j} + \text{h.c.} \right).$$

Importantly, the Ising coupling (1) is *not* affected by this transformation, $H_{12}^{\text{Ising}} = U_\gamma H_{12}^{\text{Ising}} U_\gamma^\dagger$.

For two special values of the transformation parameter γ the Emery–Kivelson transformation results in particularly interesting forms of the Hamiltonian. First consider the case when $\gamma = \sqrt{2}$. The exponents in the spin flip term of (10) then vanish and \tilde{H}_j^K can be cast into the form of the spin-boson Hamiltonian (5). We can now easily identify the coupling constants, $\Delta = \frac{J_\perp}{\pi a}$, $\lambda_k = \left(\frac{J_z}{\sqrt{2}\pi} - \sqrt{2}v_F \right) \sqrt{\frac{2\pi k}{L}}$, $\omega_k = v_F k$ and b_{qj} are the Fourier components of $\partial_x \phi_{sj}(x)$ with $\phi_{sj}(x) = -\sum_{k>0} \sqrt{\frac{2\pi}{kL}} \left(-ib_{kj} e^{-ikx} + ib_{kj}^\dagger e^{ikx} \right) e^{-ka/2}$. The linear dispersion and the form of the coupling λ_q result in a ohmic form of the spectral function $J(\omega) = 2\alpha \omega e^{-\omega/2\omega_c}$ with a strength

$$\alpha = (J_z \rho - 1)^2, \quad (11)$$

where ρ is the density of states, $\rho = 1/(2\pi v_F)$.

The single-impurity Kondo temperature has in general a power law dependence on the “tunneling rate” J_\perp ,

$$T_K^{(1)} \propto J_\perp^{\frac{1}{1-\alpha}} \quad (\text{for } J_\perp \ll J_z), \quad (12)$$

with α introduced above.

D. Generalized Anderson impurity model

Applying the Emery–Kivelson transformation with $\gamma = \sqrt{2}-1$ results in exponentials in (10) having the same form as in the bosonization identity (7) and can therefore be expressed as fermions Ψ_j . The refermionized Hamiltonian can be identified with a generalized resonant-level model^{26,27}

$$H_j^{\text{RL}} = H_0[\Psi_j] + V \left(d_j^\dagger \Psi_j(0) + \text{h.c.} \right) \quad (13) \\ + W \left(d_j^\dagger d_j - \frac{1}{2} \right) : \Psi_j^\dagger(0) \Psi_j(0) :$$

where $S_j^z = d_j^\dagger d_j - \frac{1}{2}$, $V = \frac{J_\perp}{\sqrt{2}\pi a}$ and $W = \sqrt{2}J_z - (\sqrt{2}-1)/\rho$. Ψ and d are fermionic operators, where Ψ represents solitonic spin excitations of the original conduction band, and d describes the spin degree of freedom of the impurity. The coupling W vanishes for $J_z \rho = 1 - 1/\sqrt{2}$ (or $\alpha = 1/2$ for the spin-boson model), the so-called Toulouse point of the Kondo model;²⁸ in this case Eq. (13) reduces to the conventional resonant-level model. Furthermore, $W < 0$ for isotropic small Kondo couplings, $J_z = J_\perp \ll D$.

In the new variables the Ising interaction takes the form $K_z(d_1^\dagger d_1 - \frac{1}{2})(d_2^\dagger d_2 - \frac{1}{2})$. If we interpret the bath index $j = 1, 2$ as a pseudospin index $\sigma = \uparrow, \downarrow$, we can identify the total Hamiltonian (3) with a generalized single-impurity Anderson model

$$H^A = H_0[\Psi_\sigma] + V \sum_\sigma \left(d_\sigma^\dagger \Psi_\sigma(0) + \text{h.c.} \right) + K_z \bar{n}_{d\uparrow} \bar{n}_{d\downarrow} \\ + W \sum_\sigma \bar{n}_{d\sigma} : \Psi_\sigma^\dagger(0) \Psi_\sigma(0) : \quad (14)$$

with $\bar{n}_{d\sigma} = d_\sigma^\dagger d_\sigma - \frac{1}{2}$. In this representation, the Ising interaction translates to a local Coulomb repulsion, and W corresponds to an interaction of the localized level d_σ with the surrounding electrons. In the limit $K_z = 0$ the Hamiltonian describes the extensively studied x-ray threshold problem.²¹ On the other hand, at the Toulouse point where $W = 0$, the standard impurity Anderson Hamiltonian is recovered. For large K_z the d level is mainly singly occupied; its “spin” σ corresponds precisely to the pseudospin degree of freedom of the original mini-domain. Note that the particle–hole symmetry of the effective Anderson model corresponds to the symmetry under a rotation by π around the x -axis in spin space for the original model.

The mapping of the original two-impurity model onto the generalized Anderson model (14) is one of the central

results of our paper, and will be extensively used in the numerical study of the phase diagram and the interpretation of the results.

E. Parameter mapping via phase shifts

It is important to note that the precise relation of the three models H^{SB} , H^K , and H^A depends on the cutoff structure, i.e., on properties at high energies and short distances. All formulas quoted above which relate the various coupling constants are actually only valid within the cutoff scheme underlying bosonization. However, it is generally believed that all three models are equivalent independent of the cutoff structure, as long as one considers only the universal low-energy properties in a regime where K_z and $T_K^{(1)}$ are much smaller than any other scale.

We consider now the (non-universal) mapping of model parameters within different cutoff schemes. For small values of J_\perp (or Δ and V) it is possible to calculate the precise mapping by investigating the perturbation theory in J_\perp , Δ , and V , respectively using the fact that all three models map onto a Coulomb gas^{22,23,29} – we will not attempt this here because it is difficult to do it analytically for an arbitrary cutoff scheme. However, the mapping of J_z , W , and α can be obtained directly by matching the conduction electron phase shifts in the limit $J_\perp, V = 0$, as phase shifts are measurable low-energy properties.

In the Kondo model (4), we denote the scattering phase shift for antiparallel conduction electron and impurity spins by δ_{J_z} ; for parallel spins the phase shift is then $-\delta_{J_z}$. Analogously, the phase shift in the resonant-level model (13) is δ_W if the d -level is unoccupied and $-\delta_W$ if the d -level is occupied. For a clear distinction, here and in the following we denote by ρ_F a density of states of a fermionic band with finite cutoff, whereas ρ refers to a density of states within the cutoff scheme underlying bosonization. In the latter scheme, the phase shifts defined above are directly proportional to the coupling constants, $\delta_{J_z} = \pi J_z \rho / 2$ and $\delta_W = \pi W \rho / 2$, where the density of states $\rho = 1/(2\pi v_F)$. If one uses instead a model where the high-energy cutoffs arise from a band-structure, one obtains $\delta_{J_z} = \arctan \frac{(-J_z/2)\text{Im}g_{00}(0)}{1 - (-J_z/2)\text{Re}g_{00}(0)}$, where $g_{00}(\omega) = \sum_k \frac{1}{\omega - \epsilon_k + i0^+}$ is the local Green's function of the electrons. In case of particle-hole symmetric bands, $g_{00}(0) = -i\pi\rho_F$, this relation simplifies to

$$\delta_{J_z} = \arctan[\pi J_z \rho_F / 2]. \quad (15)$$

Similarly, W in (14) induces for $V = 0$ a phase shift $\delta_W = \arctan[\pi W \rho_F / 2]$. Matching the various models by their phase shifts, the relation $W\rho = \sqrt{2}J_z\rho - (\sqrt{2} - 1)$ derived within bosonization, translates into

$$\delta_W = \arctan[\pi W \rho_F / 2] = \delta_{J_z} \sqrt{2} - \frac{\pi}{2}(\sqrt{2} - 1). \quad (16)$$

Note that this equation is only valid for small J_\perp and V .

III. STRONG-COUPLING ANALYSIS

In this section we analyze the behavior of the system for small $T_K^{(1)}/K_z$. After presenting a general argument for the existence of a phase transition, we discuss the resulting physics in terms of the generalized Anderson model (14). Interestingly, two *different* strong-coupling limits emerge which will be described in Secs. III C and III D. As detailed below, both strong-coupling limits display a phase transition of the Kosterlitz–Thouless type. Furthermore, the limits will be shown to commute, and the physical regimes are smoothly connected.

A. Effective Hamiltonian

To investigate the phase diagram sketched in Fig. 1 we consider first the limit of $|K_z| \rightarrow \infty$. We can restrict the considerations to $K_z \rightarrow +\infty$, as results for $K_z \rightarrow -\infty$ are similar because the z -component of the total spin is conserved separately for the “1” and “2” subsystems.

In the limit $K_z \rightarrow +\infty$ the two impurity spins form an antiferromagnetic mini-domain, with configurations $|\uparrow\downarrow\rangle$ and $|\downarrow\uparrow\rangle$. No fluctuations can occur for $K_z = \infty$ (or $J_\perp = 0$), therefore the ground state of the full system is a doublet.

We now set up a perturbation theory in the small parameter J_\perp/K_z , by deriving an effective Hamiltonian in the $\{|\uparrow\downarrow\rangle, |\downarrow\uparrow\rangle\}$ subspace of the impurities. The lowest process connecting the two states $|\uparrow\downarrow\rangle, |\downarrow\uparrow\rangle$ is of order $\mathcal{O}(J_\perp^2/K_z)$. Thus the effective Hamiltonian in the strong Ising-coupling limit reads

$$H_{\text{eff}}^K = H_{\text{eff},0}^K + H_{\text{eff}}^{\text{flip}} \quad (17)$$

where $H_{\text{eff},0}^K$ is given by $H_1^K + H_2^K$ with the perpendicular Kondo coupling set to zero, $J_\perp = 0$. Note that the size of J_z can be arbitrary. The mini-domain is flipped by the term

$$H_{\text{eff}}^{\text{flip}} = \frac{4J_\perp^2}{K_z} \left(S_1^+ S_2^- \Psi_{\downarrow 1}^\dagger \Psi_{\uparrow 1} \Psi_{\uparrow 2}^\dagger \Psi_{\downarrow 2} + \text{h.c.} \right) \quad (18)$$

with $\Psi_{\alpha i} = \sum_k c_{k\alpha i}$. The zero-temperature stability of the frozen mini-domain now depends on whether the operator $H_{\text{eff}}^{\text{flip}}$ is relevant in the renormalization group sense.

Since $H_{\text{eff}}^{\text{flip}}$ is comprised of four electron operators, its bare (tree-level) scaling dimension is negative, $\dim[H_{\text{eff}}^{\text{flip}}]_{\text{tree}} = -1$. This might suggest that the doublet ground state with residual entropy $\ln 2$ is stable. However, in the present problem $H_{\text{eff}}^{\text{flip}}$ acquires an anomalous scaling dimension which modifies this conclusion. This can be understood as follows: For large J_z a flip of the mini-domain suddenly changes the phase shifts of all electrons in the leads, thus exciting an infinite number of particle-hole pairs. This is the well-known orthogonality catastrophe,³⁰ leading to an anomalous long-time

response of the electrons. In the presence of a sharp Fermi edge this results in a so-called x-ray edge singularity which is reflected in an anomalous scaling dimension of $H_{\text{eff}}^{\text{flip}}$ (18).

In the following we will determine this scaling dimension using Hopfield's rule of thumb,³¹ and identify the critical J_z where the $H_{\text{eff}}^{\text{flip}}$ becomes relevant, resulting in “quantum-melting” of the frozen mini-domain.

To adjust the Fermi sea to a new ground state after the domain has flipped once, a certain amount of charge Δn has to flow to infinity. Hopfield noticed that collective response of a Fermi sea depends in the long-time limit only on this Δn : the corresponding correlation function decays as $t^{-(\Delta n)^2}$. In our problem, we have to consider four different Fermi surfaces ($j = 1, 2, \sigma = \uparrow, \downarrow$) each contributing independently.

A domain flip is induced by the operator $A = S_1^+ S_2^- \Psi_{\downarrow 1}^\dagger \Psi_{\uparrow 1} \Psi_{\uparrow 2}^\dagger \Psi_{\downarrow 2}$. According to Hopfield's rule of thumb, the correlation function in the *absence* of domain flips is then given by

$$\langle A^\dagger(t)A(0) \rangle_{H_{\text{eff},0}^K} \sim t^{-\alpha}, \quad (19)$$

where

$$\alpha = \sum_{j=1,2;\sigma=\uparrow,\downarrow} \Delta n_{j\sigma}^2. \quad (20)$$

The transferred charges $\Delta n_{j\sigma}$ are easily obtained from the phase shifts using Friedel's sum rule. For example, a spin flip induced by A changes the phase of the down electrons in bath 2 from δ_{J_z} to $-\delta_{J_z}$ which corresponds according to Friedel's sum rule to a charge transfer of $2\delta_{J_z}/\pi$. Furthermore, the annihilation operator $\Psi_{\downarrow 2}$ eliminates one charge and the total charge transfer in this channel is given by $\Delta n_{\downarrow 2} = 2\delta_{J_z}/\pi - 1$. Similar arguments give $\Delta n_{\uparrow 2} = -\Delta n_{\uparrow 1} = \Delta n_{\downarrow 1} = -\Delta n_{\downarrow 2}$. Therefore, the exponent α is given by $\alpha = 4 \left(\frac{2\delta_{J_z}}{\pi} - 1 \right)^2$. This result can also be verified explicitly by bosonization following Schotte and Schotte.³²

From Eq. (19), we can directly read off the anomalous scaling dimension of the domain-flip Hamiltonian (18) with respect to the “frozen-domain” fixed point:

$$\dim[H_{\text{eff}}^{\text{flip}}] = 1 - \frac{\alpha}{2} = 1 - 2 \left(\frac{2\delta_{J_z}}{\pi} - 1 \right)^2. \quad (21)$$

Here, the first term arises from the engineering dimension of $H_{\text{eff}}^{\text{flip}}$. For small scattering phase shifts $\dim[H_{\text{eff}}^{\text{flip}}]$ is negative, i.e., the domain flip Hamiltonian is irrelevant and the doubly degenerate “frozen-domain” fixed point described by $H_{\text{eff},0}^K$ is stable. Domain flips become relevant for $\delta_{J_z} > \delta_T$ with

$$\delta_T = \frac{\pi}{2} \left(1 - \frac{1}{\sqrt{2}} \right). \quad (22)$$

Beyond δ_T the fluctuations of the mini-domain grow towards low energies giving rise to a new phase – in this

regime the pseudospin describing the mini-domain is still well defined, but is ultimately screened at low energies. The special value of δ_T is well-known as the Toulouse point of the single-impurity Kondo Hamiltonian.³³

We have thus established the existence of a phase transition in the limit of $J_\perp/K_z \ll 1$ which is accessed by varying J_z . In the bosonization cutoff scheme, the critical value is $\rho J_z^{\text{cr}} = 1 - 1/\sqrt{2}$ corresponding to the Toulouse point of the individual Kondo impurities in the original model (3).

B. Relation to the generalized single-impurity model

What are the properties of this “fluctuating mini-domain” and what is the nature of the quantum phase transition separating the two phases? This question can be tackled within the generalized Anderson model (14).

According to Eq. (16) the coupling W in (14) vanishes for $\delta_{J_z} = \delta_T$, i.e., at the Toulouse point. This does, however, not necessarily imply that W can be treated as a small parameter in the vicinity of the Toulouse point. Rather, it is important to realize that two *different* strong-coupling limits emerge, depending on the order of limits taken in parameter space:

(i) If we consider the limit $W \rightarrow 0$ at fixed small J_\perp , then the critical K_z will diverge according to the analysis above. In this case, K_z is the largest scale, whereas J_\perp and V can be treated as perturbations.

(ii) Alternatively, we can take $J_\perp \rightarrow 0$ at fixed small $W < 0$. Apparently, the critical K_z will *vanish* (although $K_z/T_K^{(1)} \gg 1$), and a strong-coupling treatment has to consider that W is a large scale.

Both limits correspond to physical situations. However, the scaling limit, discussed at the beginning of Sec. II and employed in plotting the phase diagram of Fig. 1, is reached by taking $J_\perp \rightarrow 0$ at fixed J_z and $T_K^{(1)}/K_z$, corresponding to the case (ii) above. More generally, in a three-dimensional phase diagram which involves a third axis labelled J_\perp in addition to the ones shown in Fig. 1, case (i) applies for any finite J_\perp in a certain vicinity of the Toulouse point, before the behavior crosses over to case (ii) – this crossover scale vanishes in the universal limit $J_\perp \rightarrow 0$.

We will now analyse both cases separately – interestingly the two limits will turn out to commute.

C. $W \rightarrow 0$ at fixed V

Assuming that K_z is the largest scale in the problem, which corresponds to a strong local Coulomb repulsion on the impurity site of the generalized Anderson model, we can directly map it onto an anisotropic Kondo model. With $\bar{n}_{\Psi\sigma} =: \Psi_\sigma^\dagger(0)\Psi_\sigma(0)$ and $\mathbf{S} = \frac{1}{2}d_\alpha^\dagger \boldsymbol{\sigma}_{\alpha\beta} d_\beta$, we can rewrite $W \sum_\sigma \bar{n}_{d\sigma} \bar{n}_{\Psi\sigma} = W S_z (\bar{n}_{\Psi\uparrow} - \bar{n}_{\Psi\downarrow}) + \frac{W}{2} (\bar{n}_{d\uparrow} +$

$\bar{n}_{d\downarrow})(\bar{n}_{\Psi\uparrow} + \bar{n}_{\Psi\downarrow})$. As charge fluctuations are frozen out for large K_z , the last term can be omitted, $\bar{n}_{d\uparrow} + \bar{n}_{d\downarrow} = 1$, and we obtain

$$H_{\text{eff}}^A = H_0[\Psi_\sigma] + \sum_{n\alpha\beta} J_n^{\text{eff}} S^n \Psi_\alpha^\dagger(0) \sigma_{\alpha\beta}^n \Psi_\beta(0), \quad (23)$$

with $J_n^{\text{eff}} = (J_\perp^{\text{eff}}, J_\perp^{\text{eff}}, J_z^{\text{eff}})$ where

$$J_\perp^{\text{eff}} = \frac{4V^2}{K_z}, \quad J_z^{\text{eff}} = \frac{4V^2}{K_z} + W. \quad (24)$$

Spin-up and spin-down in this Hamiltonian correspond to the two states of the mini-domain. The phase diagram of (23) is well known: when J_z^{eff} is increased from negative values towards zero (keeping $J_\perp^{\text{eff}} \neq 0$ fixed) one observes a quantum phase transition from a ferromagnetic regime with $\ln 2$ residual entropy to a Fermi-liquid phase where the spin is quenched, see Fig. 3. The $S_0 = \ln 2$ phase can obviously be identified with our “frozen mini-domain”. It is stable for $J_z^{\text{eff}} < -|J_\perp^{\text{eff}}|$ or $W < W_c$ with

$$W_c = -\frac{8V^2}{K_z}. \quad (25)$$

For $K_z \rightarrow \infty$ or $V \rightarrow 0$, the phase transition is located at $W_c = 0$ or equivalently $\delta_{J_z} = \delta_T$ as anticipated above. Eq. (25) is the *exact* result for the phase boundary for $K_z \rightarrow \infty$, provided that V and W are mapped onto J_\perp and J_z as described in Sec. II. We note again that the limit considered here does *not* correspond to the universal limit $J_\perp \rightarrow 0$, because this would give $K_z^{cr} \rightarrow 0$ at any fixed W .

D. $V \rightarrow 0$ at fixed W

Anticipating that $K_z^{cr} \rightarrow 0$ in this limit, we need to consider a problem where W is a large local energy scale. Interestingly, at $K_z = 0$ and $V = 0$ the four impurity states are degenerate even in the presence of W because of overall particle-hole symmetry. This degeneracy is lifted by K_z which (as above) favors the impurity states $|\uparrow\downarrow\rangle$ and $|\downarrow\uparrow\rangle$ (assuming $K_z > 0$).

We proceed with an analysis similar to the usual Schrieffer-Wolff transformation, now in the presence of a large W . As usual, hopping processes of second order in V produce an effective pseudospin interaction between the impurity and the conduction band. However, as the impurity occupation in the intermediate states is different from that of initial and final states, the intermediate state physics involves an x-ray edge singularity due to the sign change of the strong potential scatterer W .

Analyzing the matrix elements, we find x-ray edge behavior which is cutoff by K_z , i.e., the effective generated Kondo couplings are of the form $V^2/K_z^{1-\beta}$ where

$$\beta = -2\frac{2}{\pi}\delta_W - \left(\frac{2}{\pi}\delta_W\right)^2 \quad (26)$$

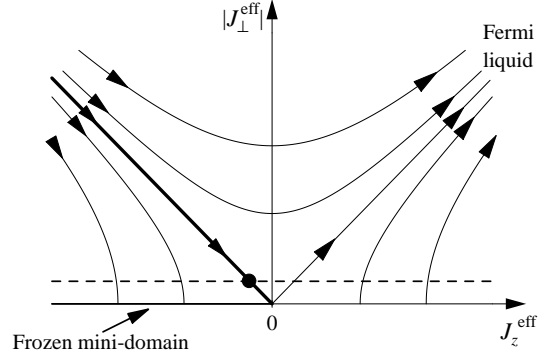


FIG. 3: Schematic renormalization-group flow of the effective Kondo model (23),^{1,23} describing the screening of the mini-domain pseudospin in the limit of large K_z . Here, $J_z^{\text{eff}} = 0$ corresponds to the Toulouse point of the original Kondo model. The Fermi-liquid fixed point is characterized by pseudospin screening; the frozen-mini-domain phase corresponds to a *line of fixed points* with unscreened pseudospin. The thick line denotes the phase boundary, given by $J_z^{\text{eff}} = -|J_\perp^{\text{eff}}|$. Variation of J_z around the Toulouse point in the original model (at fixed J_\perp and K_z) corresponds to a parameter variation in the effective model as shown by the dashed line; the dot is the transition point. The transition is in the Kosterlitz-Thouless universality class.

where $\delta_W = \pi W \rho / 2$ is the phase shift from W .

The detailed derivation of the generalized Schrieffer-Wolff transformation is given in App. A. Finally, one arrives at an effective Kondo model of the form (23), but now with couplings

$$J_\perp^{\text{eff}} = \frac{4V^2 f_\perp(\delta_W)}{K_z^{1-\beta} \Lambda^\beta}, \quad J_z^{\text{eff}} = \frac{4V^2 f_z(\delta_W)}{K_z^{1-\beta} \Lambda^\beta} + W \quad (27)$$

where Λ is of the order of the band cutoff, and both f_\perp and f_z are smooth, dimensionless functions of δ_W with

$$\lim_{W \rightarrow 0} f_\perp(\delta_W) = f_\perp(0) = 1, \quad \lim_{W \rightarrow 0} f_z(\delta_W) = f_z(0) = 1. \quad (28)$$

As above, the model shows a Kosterlitz-Thouless phase transition in this effective Kondo model occurs at the line $J_\perp^{\text{eff}} = -|J_z^{\text{eff}}|$, i.e.

$$W = -\frac{4V^2[f_\perp(\delta_W) + f_z(\delta_W)]}{K_z^{1-\beta} \Lambda^\beta} \quad (29)$$

where β is a function of W according to $1 - \beta = 2(1 - \alpha)$ with $\alpha = (J_z \rho - 1)^2$ as introduced above. To obtain an explicit relation between W , V , and K_z in the vicinity of the Toulouse point, we expand in W . Dropping additive logarithmic corrections, we have

$$W^{\frac{1}{1-\beta}} \approx W, \quad \Lambda^\beta \approx 1. \quad (30)$$

With this and (28) we can re-write Eq. (29) as

$$W = -8 \frac{V^{\frac{1}{1-\alpha}} \Lambda^{\frac{1-2\alpha}{1-\alpha}}}{K_z} \quad (31)$$

which is *smoothly* connected to the result (25) obtained in the limit $W \rightarrow 0$ of Sec. III C.

As announced, the critical K_z for fixed W depends only on $T_K^{(1)} \propto V^{\frac{1}{1-\alpha}} \Lambda^{\frac{1-2\alpha}{1-\alpha}}$. To fix the prefactor, we first have to *define* $T_K^{(1)}$ for an asymmetric Kondo model. This is best done using a physical observable like the impurity specific heat coefficient $\gamma = \lim_{T \rightarrow 0} C_{\text{imp}}/T$ of the anisotropic single-impurity Kondo model. We employ

$$T_K^{(1)} \equiv w \frac{\pi^2}{3} \gamma^{-1}, \quad (32)$$

where $w = 0.4128$ is the Wilson number.¹ At the Toulouse point, $\alpha = 0$, one easily finds $\gamma = 1/(3\rho_F V^2)$. Thus, for $W \rightarrow 0$ we obtain:

$$\rho_F W = -\frac{8}{w\pi^2} \frac{T_K^{(1)}}{K_z^{cr}} \approx -1.964 \frac{T_K^{(1)}}{K_z^{cr}}. \quad (33)$$

For particle-hole symmetric bands, this can be re-written using Eqs. (15) and (16) into:

$$\begin{aligned} \frac{T_K^{(1)}}{K_z^{cr}} &= \frac{\rho_F w \pi^2 \sqrt{2} \sin^2(\frac{\pi}{2\sqrt{2}})}{8} (J_z^{cr} - J_z) \\ &\approx 0.578 \rho_F (J_z^{cr} - J_z) \end{aligned} \quad (34)$$

valid for $J_z \rightarrow J_z^{cr}$.

Concluding this analysis, we have shown that also in the limit $V \rightarrow 0$ (keeping W fixed) the effective Anderson model (14) can be mapped onto an effective Kondo model, which describes the screening of the mini-domain pseudospin. The phase transition is in the Kosterlitz–Thouless universality class. The two strong-coupling limits are adiabatically connected, as the involved impurity states and transitions are similar in both cases; in addition the equations for the phase boundaries (25) and (31) match.

From the mapping to the anisotropic Kondo model we can also identify the “fluctuating mini-domain” regime with a Fermi-liquid phase. Here, the pseudospin is screened below the Kondo temperature, T^* , of the effective Kondo model (23). Importantly, the Fermi sea of the effective model is formed by solitonic spin excitations of the original model (3) – this will strongly influence the conductance through the system as discussed in Sec. VII. At the Toulouse point, we can estimate $T^* \sim \min(K_z, D) \exp[-|K_z|/(8V^2 \rho_F)]$. Close to the quantum phase transition, reached for $K_z/V^2 \rightarrow 0$ at the Toulouse point, T^* is exponentially small. Similarly, for finite K_z^{cr} and $K_z \lesssim K_z^{cr}$, one expects for a Kosterlitz–Thouless transition the behavior³⁴

$$T^* = a e^{-b/\sqrt{K_z^{cr}-K_z}}, \quad (35)$$

where a is a function of $T_K^{(1)}$ and J_z ; this form will actually be used to fit the numerical data of Sec. IV.

At the Toulouse line, one can investigate the crossover from the “fluctuating mini-domain” regime to the regime

with Kondo-screened spins at $K_z = 0$ (dashed crossover line in Fig. 1). As our model is equivalent to an Anderson impurity model (14), this crossover is equivalent to the well-known Anderson model crossover from mixed-valence to Kondo behavior. This crossover takes place at $K_z \sim V^2 \rho_F$, i.e., when $T_K^{(1)}/K_z$ is of order $\mathcal{O}(1)$. Similarly, one finds for $J_z \rightarrow \infty$ that this crossover is located at $T_K^{(1)} \sim J_\perp \sim K_z$, and furthermore for $J_z \rightarrow 0$ one also expects this crossover at $K_z \sim T_K^{(1)}$ (as no other low-energy scale exists in this regime). We therefore conclude that the dashed crossover line in Fig. 1 is always located at $T_K^{(1)}/K_z \sim \mathcal{O}(1)$.

The schematic RG flow of the effective Kondo model, shown in Fig. 3, illustrates the behavior of the Ising-coupled two-impurity model in the strong-coupling regime. Three observations are important: (i) Both the $S_0 = \ln 2$ frozen-domain phase and the $S_0 = 0$ Fermi-liquid phase are stable to small perturbations – this conclusion is in agreement with the analysis of Ref. 20. (ii) The $S_0 = \ln 2$ phase corresponds to a *line* of RG fixed points. (iii) The two phases are separated by a Kosterlitz–Thouless transition, characterized by logarithmic rather than power-law behavior of thermodynamic observables.

So far, the conclusions above mainly apply to the vicinity of the Toulouse point of the single-impurity model, i.e., for strongly anisotropic Kondo coupling. In the next section we will present numerical results which strongly support that the above picture is valid over the whole phase diagram. In particular, we shall show that the phase transition is of Kosterlitz–Thouless type even in the case of isotropic Kondo couplings. Furthermore, no other phase transition (than the one indicated in Fig. 1) occurs; this implies that the Fermi liquid formed by the fluctuating mini-domain is adiabatically connected to the Fermi liquid of two individually Kondo-screened spins, realized in the limit $K_z \ll T_K^{(1)}$.

IV. NUMERICAL RENORMALIZATION GROUP ANALYSIS

In this section, we turn to a numerical investigation of the model of Ising-coupled impurities using the numerical renormalization group (NRG) technique.² In principle, an investigation of the original two-impurity model (3) is possible – however, the required two bands of spinful fermions are computationally demanding within NRG, and results are significantly less accurate compared to the NRG treatment of single-band impurity models.

Therefore, we have decided to study the generalized Anderson model of Eq. (14), obtained after bosonization and refermionization of the original model. Featuring only one band of spinful conduction electrons, it allows high-accuracy numerical simulations down to lowest energy scales and temperatures.

A. Parameters

In the following, we will show numerical results for the generalized Anderson model (14), for a rectangular particle-hole symmetric fermionic band of width $D = 2\sqrt{2}$, and different values of the hybridization V , density interaction W , and on-site repulsion K_z – note that K_z is identical to the original Ising interaction between the two impurities, whereas V and W are related to J_\perp and J_z as detailed in Sec. II. In particular, W measures the deviation from the Toulouse point. According to Eq. (16), valid for small V , $J_z = 0$ corresponds to $W\rho_F = -(2/\pi)\tan[\pi(\sqrt{2}-1)/2] \approx -0.48$. Similarly, large negative values of W , i.e., $W \rightarrow -\infty$, correspond to $\rho J_z = 1 - \sqrt{2} = -\sqrt{2}(\rho J_z)_{\text{Toulouse}}$ with ρJ_z here defined in the bosonization cutoff scheme.

The mapping between V and J_\perp (which are simply proportional) can be achieved via the Kosterlitz–Thouless transition line for a single impurity: This line, where $T_K^{(1)}$ vanishes, is given by $J_z = -|J_\perp|$. Using NRG, we have numerically determined a few points on this line, characterized by parameters V and W in the model formulation (14) with $K_z = 0$ – note that this involves an extrapolation of $T_K(V)$ to $T_K = 0$. With the mapping between W and ρJ_z established above, we find for the employed parameters the correspondence $\rho J_\perp \approx 0.38V$, valid for small V .

Within NRG, the bath density of states is discretized on a logarithmic grid, with a discretization parameter Λ , i.e., the energy axis is divided into intervals at points $D, D\Lambda^{-1}, D\Lambda^{-2}, \dots$. The discretized model is transformed into a semi-infinite chain form, and then diagonalized iteratively.² After each diagonalization step the lowest N_s eigenstates of the Hamiltonian are kept. Clearly, the results are “exact” in the limit $N_s \rightarrow \infty$, $\Lambda \rightarrow 1$. In practice, numerical results are monitored at fixed Λ , where convergence upon increasing the value of N_s can be readily achieved. Then, these converged numbers are extrapolated as function of Λ to $\Lambda = 1$ to obtain an estimate for the “exact” result.

Most of the NRG calculations here have employed a discretization parameter of $\Lambda = 2$, keeping $N_s = 650$ states per NRG step. For selected parameter values we have performed calculations with different Λ and N_s . For each Λ convergence w.r.t. N_s can be easily achieved, however, for some quantities the Λ dependence turns out to be rather strong. Therefore, the $\Lambda \rightarrow 1$ extrapolation has to be performed carefully, as will be detailed at the end of this Section.

The results shown below primarily correspond to the universal regime of $V \ll W, D$ and $K_z \ll W, D$; we have also performed some calculations in the regime $K_z \gg W$ (not shown) with results consistent with the analysis of Sec. III C.

B. Results for RG flow and entropy

In Fig. 4 we show NRG flow diagrams displaying the energies of a few low-lying many-body eigenstates as function of the number of NRG steps. The data in Fig. 4a clearly show that for small values of K_z the same fixed point is reached for any V and W – this fixed point can be identified with the Fermi-liquid phase, which is in particular also reached for $K_z = 0$. Therefore, the Fermi-liquid regime of two separately Kondo-screened impurities is adiabatically connected to the “fluctuating mini-domain” regime which can be characterized by pseudospin screening below the collective Kondo temperature T^* . In Fig. 4b flow diagrams for larger values of K_z are shown – here the fixed points reached at low energies are very similar for different parameter sets, but not identical – this is consistent with the notion of a line of fixed points with $\ln 2$ residual entropy.

It is important to emphasize that no additional fixed point is observed for $K_z \approx K_z^{cr}$, which could possibly correspond to a critical fixed point. This clearly shows that the quantum phase transition in our problem is not associated with standard critical behavior, but indicates that it is of the Kosterlitz–Thouless universality class.

To characterize the fixed points, we have evaluated the impurity entropy $S(T)$ using NRG. In Fig. 5 we show results for different values of W and several K_z . The discussed two-stage quenching of the entropy, occurring for $T_K^{(1)} < K_z < K_z^{cr}$, can be nicely seen in all panels – note that panel c) shows data for $W > 0$, i.e., on the right-hand side of the Toulouse point.

C. Phase boundary and phase diagram

From the NRG results for fixed values of W , V and different $K_z < K_z^{cr}$ it is possible to extract a characteristic crossover temperature T^* below which the pseudospin is screened, see above. For numerical simplicity we defined T^* through $S(T^*) = 0.4$. The dependence of T^* on K_z allows to determine K_z^{cr} where T^* vanishes. We fitted the data with $T^*(K_z) = a \exp[b/\sqrt{K_z^{cr} - K_z}]$ (35) with fit parameters a , b , K_z^{cr} , which is the form expected near a Kosterlitz–Thouless transition³⁴. The fit works excellently for all anisotropies, as shown in Fig. 6 – this is again strong support for the Kosterlitz–Thouless nature of the transition.

The single-impurity Kondo temperature, $T_K^{(1)}$ for given W and V is determined from Eq. (32), where the specific heat coefficient γ is extracted from the NRG data for $S(T)$.

Having determined both $T_K^{(1)}$ and K_z^{cr} , we are in the position to plot the phase diagram in the universal fashion indicated in Fig. 1, i.e., employing the limit $T_K^{(1)} \ll D$. The result is shown in the main panel of Fig. 7.

It is possible to make the meaning of universality more

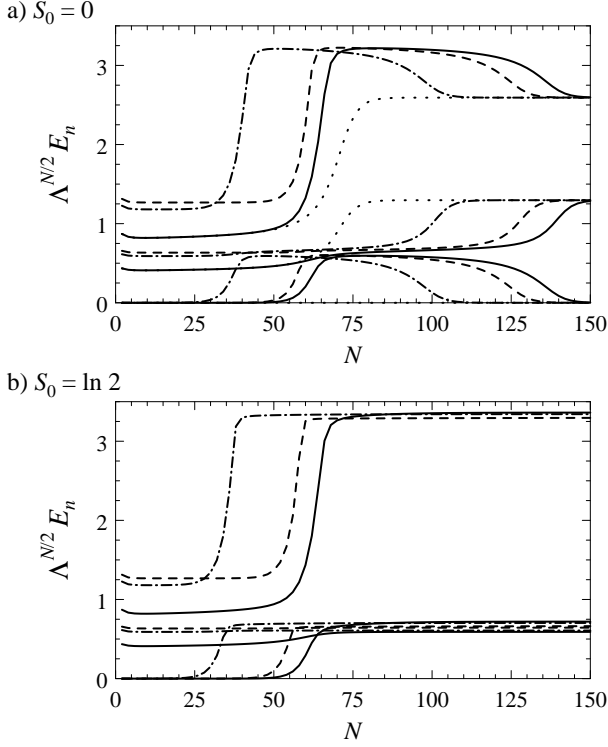


FIG. 4: NRG flow diagram for the generalized single-impurity Anderson model (14), for parameter values belonging to a) the Fermi-liquid phase with $S_0 = 0$, b) the frozen-domain phase with $S_0 = \ln 2$. Solid: $W\rho_F = -0.44$, $V = 0.075$ ($K_z^{cr} = 7.6 \times 10^{-10}$), Dash-dot: $W\rho_F = -0.10$, $V = 1.5 \times 10^{-3}$ ($K_z^{cr} = 3.4 \times 10^{-6}$), Dashed: $W\rho_F = -0.034$, $V = 1.5 \times 10^{-5}$ ($K_z^{cr} = 4.8 \times 10^{-9}$). In a) and b), K_z has been chosen slightly below and above the critical value, respectively. For all parameters, the system is in a $S = \ln 4$ regime at high temperatures (small N), in a) it flows to the $S = 0$ state by passing through a regime with $S = \ln 2$. In a), the additional dotted curves show the flow for $W\rho_F = -0.44$, $V = 0.075$, and $K_z = 0$. The $W\rho_F$ values span a large range of anisotropies; nevertheless, the $S = 0$ fixed point is unique, and the finite-temperature crossover is universal for the curves close to K_z^{cr} . Panel b) nicely shows that $S = \ln 2$ actually corresponds to a line of fixed points. NRG parameters are $\Lambda = 2$ and $N_s = 650$.

precise: so far we have distinguished the parameter sets by their value of J_z (or W), leading to different values of $T_K^{(1)}/K_z^{cr}$. Within the RG treatment of Yuval and Anderson²⁹ for the single-impurity Kondo model, it is easily seen that we can expect identical low-energy behavior for two single-impurity models if the initial parameters place the two models on the same RG trajectory. (The RG trajectories are identical to the ones shown in Fig. 3.) Therefore, the correct parameter for the horizontal axis of our phase diagram is a parameter labelling the RG trajectories, i.e., a proper RG invariant. Note that for $J_z > 0$ and $J_\perp \rightarrow 0$, J_z can be used as such a label – this is what we have done so far. A proper RG invariant

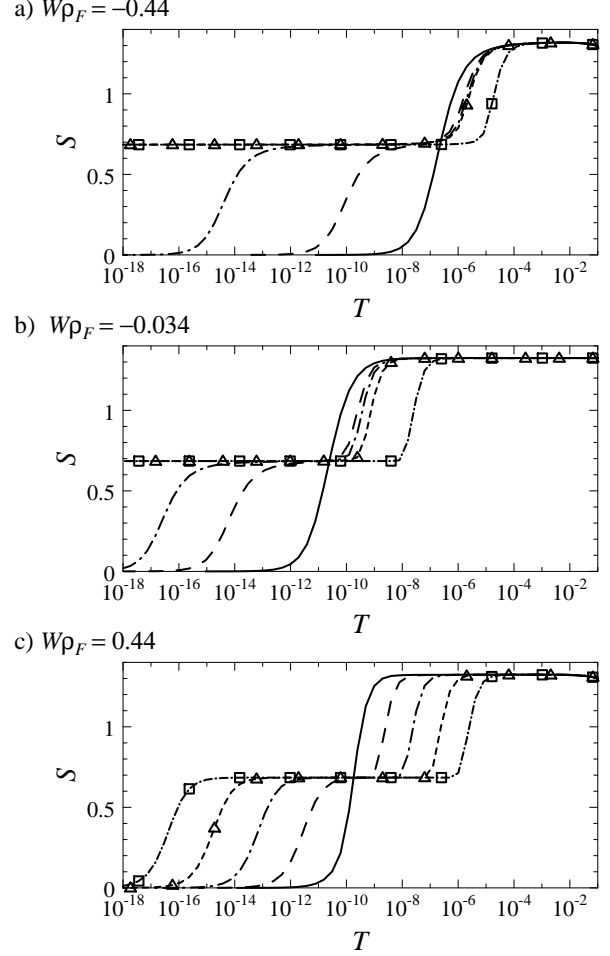


FIG. 5: Temperature evolution of the impurity entropy calculated by NRG for the generalized single-impurity Anderson model (14) for different anisotropies of the Kondo coupling. In the “frozen mini-domain” phase the residual entropy is $\ln 2$ while it vanishes for $K_z < K_z^{cr}$. For $T_K^{(1)} \gg K_z$ (solid curves), the high-temperature $\ln 4$ entropy is quenched in a single step, whereas two-stage screening occurs for $T_K^{(1)} < K_z < K_z^{cr}$. a) $W\rho_F = -0.44$, $V = 0.15$ ($K_z^{cr} = 1.5 \times 10^{-5}$), close to isotropic Kondo coupling. K_z is: Solid 0, long-dash 10^{-5} , long-dash-dot 1.3×10^{-5} , short-dash 1.5×10^{-5} , short-dash-dot 10^{-4} . b) $W\rho_F = -0.034$, $V = 1.5 \times 10^{-5}$ ($K_z^{cr} = 4.8 \times 10^{-9}$), i.e., close to the Toulouse point of the individual Kondo impurities. The K_z values are: Solid 0, long-dash 10^{-9} , long-dash-dot 1.5×10^{-9} , short-dash 3×10^{-9} , short-dash-dot 10^{-7} . c) $W\rho_F = 0.44$, $V = 1.5 \times 10^{-7}$, i.e., on the right-hand side of the phase diagram Fig. 1 where no phase transition occurs as function of K_z . K_z is: Solid 0, long-dash 10^{-8} , long-dash-dot 10^{-7} , short-dash 10^{-6} , short-dash-dot 10^{-5} .

is c defined by²⁹

$$c = 4(J_\perp \rho)^2 + \epsilon + 2 \ln \left(1 - \frac{\epsilon}{2} \right), \quad (36)$$

$$\epsilon = 8 \frac{\delta J_z}{\pi} - 8 \left(\frac{\delta J_z}{\pi} \right)^2,$$

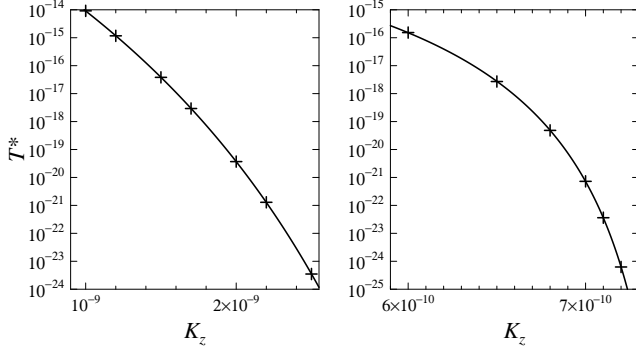


FIG. 6: Numerically determined values of $T^*(K_z)$ for $W\rho_F = -0.034$, $V = 1.5 \times 10^{-5}$ where $K_z^{cr} = 4.8 \times 10^{-9}$ (left), and $W\rho_F = -0.44$, $V = 0.075$ where $K_z^{cr} = 7.6 \times 10^{-10}$ (right); together with the exponential fit described in the text.

where $\delta_{J_z} = \pi J_z \rho / 2$ is the phase shift resulting from J_z , and we have employed the bosonization cutoff scheme here. For small values of both J_z and J_\perp , the above equations can be expanded to yield:

$$c = 4(J_\perp \rho)^2 - 4(J_z \rho)^2. \quad (37)$$

For $J_\perp \rightarrow 0$ the value of c thus depends only on J_z as anticipated; in this regime $c < 0$. The advantage of using a parametrization of the single-impurity RG flow via c is that it allows to cover the trajectories with $|J_\perp| > |J_z|$ as well, i.e., the trajectories above the isotropic line in Fig. 3; here $c > 0$.

With the parameter mapping described at the beginning of this section we have all parameters at hand and can determine the value of c from V and W . This allows to re-plot the phase diagram in a plane spanned by $T_K^{(1)}/K_z^{cr}$ and c – this is shown in the inset of Fig. 7. In particular, we can now add data points for $J_z < 0$ to the phase boundary plot, as those are characterized by a *finite* J_\perp in the limit $T_K^{(1)} \ll D$.

As mentioned above, some NRG results show a relatively strong dependence on the NRG discretization parameter Λ . Fig. 7 shows the phase diagram for $\Lambda = 2$; results for other Λ values are similar, but the $T_K^{(1)}/K_z^{cr}$ values can differ by 50% or more. Therefore, we have performed an extrapolation to $\Lambda \rightarrow 1$ for a few important quantities. A sample extrapolation is shown in Fig. 8 for the slope of the phase boundary near the Toulouse point, which was determined analytically in Sec. III – the extrapolated value of $K_z W / V^{1/(1-\alpha)}$ is consistent with the exact result in Eq. (31). We have also looked at the maximum value of $T_K^{(1)}/K_z$ of the phase boundary occurring near $J_z = 0$, this value extrapolates to $(T_K^{(1)}/K_z)_{\max} = 0.11 \pm 0.03$.

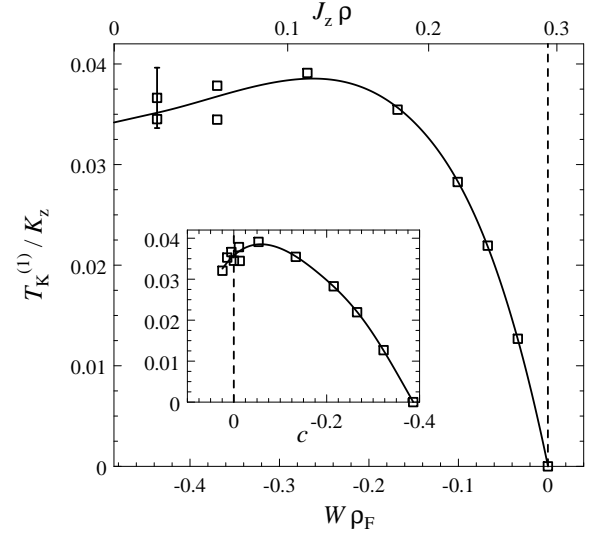


FIG. 7: Phase diagram of the generalized single-impurity Anderson model (14) deduced from NRG calculations for NRG discretization parameter $\Lambda = 2$. The vertical dashed line shows the Toulouse point of the individual Kondo impurities. Small values of V have been used to reach the universal regime $T_K^{(1)} \ll D$. Precise values of $T_K^{(1)}$ have been determined via the specific heat coefficient γ , see text. The upper horizontal axis shows the corresponding values of J_z in the bosonization cutoff scheme. The error bar shows the typical uncertainty in the numerical determination of $T_K^{(1)}/K_z^{cr}$ arising from the fits of both γ and K_z^{cr} . The inset shows the same data for $T_K^{(1)}/K_z^{cr}$, now plotted as function of the RG invariant c of the single-impurity model (36) – this plot covers the range of positive as well as negative J_z (here $c > 0$). The lines are guide to the eye only.

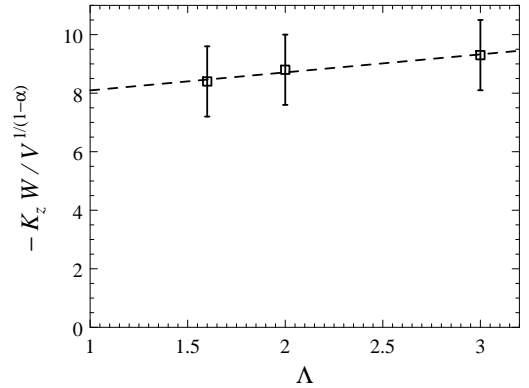


FIG. 8: Λ dependence of the slope of the phase boundary near the Toulouse point. (Λ is the NRG parameter defining the logarithmic discretization of the conduction band.) The dashed line is a linear fit. Each data point involves an extrapolation of the numerical results at finite negative W to $W \rightarrow 0$. A rather strong Λ dependence can be observed, however, the extrapolated value appears consistent with the analytical result (31).

V. FLOW EQUATIONS

In this section, we consider a different approach³⁹ to our original model of Ising-coupled Kondo impurities, which is based on the method of flow equations.³⁵ The general idea is an approximate diagonalization of each of the two Kondo impurities – the result is a resonant-level-type effective model which captures the Kondo physics in terms of a non-trivial renormalized hybridization. Taking the two Ising-coupled impurities together, we will again arrive at an effective Anderson model. Away from the Toulouse line one finds an additional weak density-density interaction. However, in contrast to Sec. IIID where we were forced to treat a similar interaction non-perturbatively to take into account x-ray edge singularities (App. A), this is not necessary here because this non-trivial physics is already contained in the fully renormalized couplings which naturally appear within the flow-equation approach. This approach allows for a systematic expansion around the Toulouse line, and the effective Hamiltonian derived in this framework in fact describes the entire phase diagram of Fig. 1 consistently.

A. Flow equation transformation

The flow equation method was first applied to the Kondo model in Ref. 36, where it was shown that it leads to an expansion around the Toulouse point. Its basic idea is to perform a sequence of infinitesimal unitary transformations on a given many-particle Hamiltonian and thereby diagonalizing it.³⁵ The expansion parameter turns out to be $\lambda_0 - 1$ with $\lambda_0 = \sqrt{2}(1 - J_z \rho) = 1 - W\rho$ (using the bosonization cutoff scheme); the Toulouse point corresponds to $\lambda_0 = 1$.

Following Ref. 36, we construct unitary transformations $U_{1,2}$ (see App. B) such that the single-impurity Hamiltonians $\tilde{H}_{1,2}^K$ from Eq. (10) become diagonal

$$H_{1,2}^{(K-\text{diag})} = U_{1,2} \tilde{H}_{1,2}^K U_{1,2}^\dagger \quad (38)$$

up to higher-order terms in our expansion around the Toulouse line. For studying the Ising-coupled Kondo impurities we therefore apply the combined unitary transformation $U = U_1 U_2$ on (3), $\tilde{H}^K = U H^K U^\dagger$, leading to

$$\tilde{H}^K = H_1^{(K-\text{diag})} + H_2^{(K-\text{diag})} + K_z \tilde{S}_1^z \tilde{S}_2^z \quad (39)$$

with $\tilde{S}_{1,2}^z = U_{1,2} S_{1,2}^z U_{1,2}^\dagger$. At the Toulouse point (39) is of course exactly equivalent to the Anderson impurity model (13) with $W = 0$ and the same mapping as used in Secs. IIC and IID: the unitary transformation $U_{1,2}$ just eliminates the hybridization coupling in the Anderson impurity model.

It was shown in Ref. 37 that the flow equation approach yields a resonant-level model (13) as an effective

model for the Kondo impurity model also away from the Toulouse point

$$H^{(RL-\text{eff})} = H_0[\Psi_j] + \sum_k \tilde{V}_k \left(d_j^\dagger \Psi_j(k) + \text{h.c.} \right), \quad (40)$$

where the $\Psi_j^\dagger(k), \Psi_j(k)$ are the creation and annihilation operators for solitonic spin excitations in momentum space. However, this resonant-level model now has a nontrivial renormalized hybridization function, $\Delta(\epsilon) \stackrel{\text{def}}{=} \sum_k \tilde{V}_k^2 \delta(\epsilon - \epsilon_k)$, with (i) $\Delta(0) = T_K^{(1)}/w\pi^2$ and nearly constant in an energy interval of order $T_K^{(1)}$ around the Fermi energy (here $\epsilon_F = 0$), and (ii) a non-trivial power-law behavior for larger energies. Furthermore, it was shown in Ref. 37 that to *leading* order in an expansion around the Toulouse line one can identify $S_j^z = d_j^\dagger d_j - 1/2$. The effective model for our system of Ising-coupled Kondo impurities is therefore an Anderson impurity model with a hybridization function of order the single-impurity Kondo scale:

$$H^{(A-\text{eff})} = H_0[\Psi_\sigma] + \sum_{k,\sigma} \tilde{V}_k \left(d_\sigma^\dagger \Psi_\sigma(k) + \text{h.c.} \right) + K_z \bar{n}_{d\uparrow} \bar{n}_{d\downarrow}. \quad (41)$$

The main feature of the flow equation method is therefore to eliminate the large coupling W in (14) by renormalizing the hybridization of the Anderson model.

However, since the flow equation transformation is an expansion in the distance $(\lambda_0 - 1)$ to the Toulouse line, we need to be careful in the transformation of S^z : The transformed \tilde{S}^z is multiplied by a possibly large parameter K_z , so that an error of order $(\lambda_0 - 1)$ in the expansion becomes multiplied by K_z , leading to additional interaction terms in (41) that can be larger than the hybridization energy scale $T_K^{(1)}$.³⁹ It are precisely these additional interactions that drive the Kosterlitz–Thouless transition between the Fermi-liquid phase and the frozen mini-domain phase for $|K_z(\lambda_0 - 1)| \gtrsim T_K^{(1)}$.

B. Corrections to the transformation of \tilde{S}^z

In App. B the flow equation solution for the single impurity Kondo model $H_{1/2}^K$ in a magnetic field h is discussed with a careful analysis of terms of order $(\lambda_0 - 1)$. Here h is the effective exchange field due to the second spin, to be described below. The transformed operator \tilde{S}_j^z takes the following form

$$\begin{aligned} \tilde{S}_j^z &= \frac{1}{2} \int dx dx' d(x) d^*(x') [\Psi_j^\dagger(x), \Psi_j(x')] \\ &\quad + \frac{1}{2} (\lambda_0 - 1) f(h) \partial_x \bar{\phi}_j(0) \end{aligned} \quad (42)$$

plus irrelevant terms (containing e.g. higher derivatives of the bosonic field) and plus higher order terms of order $(\lambda_0 - 1)^2$. The first term on the right-hand side of

Eq. (42) can be interpreted as the result of integrating out the hybridization term in (40), while the second term is a correction term not contained in the original solution in Ref. 36. $\bar{\phi}_j(0)$ denotes the bosonic spin-density field $\phi_j(x)$ without the Fourier components for energies larger than $\mathcal{O}(T_K^{(1)})$ (with respect to low-energy properties one does not need to distinguish these fields). Properties of the dimensionless function $f(h)$ are derived in App. B,

in particular $f(h) = v_F/|h| + \mathcal{O}(h^{-2})$ for $|h| \gg T_K^{(1)}$.

In the coupled system (41) we can approximate the effect of one spin on the other as a static magnetic field of strength $h = \pm K_z/2$ close to the transition. This approximation becomes asymptotically exact as one approaches the transition since the spin dynamics becomes slower and slower.

We arrive at the following Hamiltonian describing the coupled Kondo impurities in the vicinity of the transition line.

$$H^{(A-\text{eff})} \approx H_0[\Psi_\sigma] + \sum_{k,\sigma} \tilde{V}_k (d_\sigma^\dagger \Psi_\sigma(k) + \text{h.c.}) + K_z \bar{n}_{d\uparrow} \bar{n}_{d\downarrow} + (\lambda_0 - 1) \frac{K_z}{2} f(K_z/2) (\partial_x \bar{\phi}_\uparrow(0) \bar{n}_{d\downarrow} + \bar{n}_{d\uparrow} \partial_x \bar{\phi}_\downarrow(0)) \quad (43)$$

up to corrections of order $(\lambda_0 - 1)^2$.

C. The Kosterlitz–Thouless transition

Let us now focus on the case $K_z \gg T_K^{(1)}$ that is relevant for studying the phase transition in the vicinity of the Toulouse line. Using $f(h) \approx v_F/|h|$ we rewrite the Hamiltonian (43) as

$$H^{(A-\text{eff})} = H_0[\Psi_\sigma] + \sum_{k,\sigma} \tilde{V}_k (d_\sigma^\dagger \Psi_\sigma(k) + \text{h.c.}) + K_z \bar{n}_{d\uparrow} \bar{n}_{d\downarrow} + (\lambda_0 - 1) v_F ((\partial_x \bar{\phi}_\uparrow(0) + \partial_x \bar{\phi}_\downarrow(0)) \frac{1}{2} (\bar{n}_{d\uparrow} + \bar{n}_{d\downarrow}) - (\partial_x \bar{\phi}_\uparrow(0) - \partial_x \bar{\phi}_\downarrow(0)) \frac{1}{2} (\bar{n}_{d\uparrow} - \bar{n}_{d\downarrow})) . \quad (44)$$

Similar to the analysis in Sec. III C the term proportional to $\bar{n}_{d\uparrow} + \bar{n}_{d\downarrow}$ is frozen out and can be ignored, while the term proportional to $\bar{n}_{d\uparrow} - \bar{n}_{d\downarrow}$ leads to a spin-spin interaction. Since K_z is the largest energy scale in (44) with its renormalized parameters, we can map the Hamiltonian onto an anisotropic Kondo model using a Schrieffer–Wolff transformation (like in Sec. III C) and again arrive at (23)

$$H_{\text{eff}}^A = H_0[\Psi_\sigma] + \sum_{n\alpha\beta} J_n^{\text{eff}} S^n \Psi_\alpha^\dagger(0) \sigma_{\alpha\beta}^n \Psi_\beta(0) , \quad (45)$$

where now the Kondo couplings for scattering processes in the vicinity of the Fermi surface contain the renormalized parameters $\rho_F \tilde{V}^2 = T_K^{(1)}/w\pi^2$

$$\rho_F J_\perp^{\text{eff}} = \frac{4\rho_F \tilde{V}^2}{K_z} , \quad \rho_F J_z^{\text{eff}} = \frac{4\rho_F \tilde{V}^2}{K_z} - \rho_F J^{(\text{nl})} \quad (46)$$

with $\rho_F J^{(\text{nl})} = \lambda_0 - 1$. We stress that here it was *not* necessary to use the generalized Schrieffer–Wolff transformation derived in App. A as the parameters in (44) are already renormalized due to the flow equation procedure and the interactions $\propto \lambda_0 - 1$ are only effective at low energies. The additional spin-spin interaction $J^{(\text{nl})}$ is ferromagnetic for couplings to the right-hand side of the Toulouse line $\lambda_0 > 1$. This leads to a critical coupling for the Kosterlitz–Thouless transition to the frozen

mini-domain phase

$$K_z^{cr} = \frac{8\rho_F \tilde{V}^2}{\lambda_0 - 1} = \frac{8\tilde{V}^2}{-W} \quad (47)$$

or using Eq. (32)

$$\rho_F K_z^{cr} = \frac{8}{w\pi^2} \frac{T_K^{(1)}}{-W} = 1.964 \frac{T_K^{(1)}}{-W} \quad (48)$$

in exact agreement with the NRG results (Fig. 8) and the strong-coupling analysis Eq. (33) in Sec. III D.

Since the flow equation approach leads to a renormalized effective Hamiltonian, one can also use it to derive the entire phase diagram like in Fig. 7. If one neglects the same higher order terms $(\lambda_0 - 1)^2$ as before, one finds the following result for the critical coupling

$$\rho_F K_z^{cr} = \frac{8}{w\pi^2} \frac{T_K^{(1)}}{-W} (1 - \Lambda'(0)) , \quad (49)$$

which simply results from a Schrieffer–Wolff transformation of an Anderson model with an on-site repulsion K_z and a hybridization $\Delta(\epsilon)$ which enters as $T_K^{(1)}$. Here

$$\Lambda(\omega) = \frac{1}{\pi} P \int d\epsilon \frac{\Delta(\epsilon)}{\omega - \epsilon} \quad (50)$$

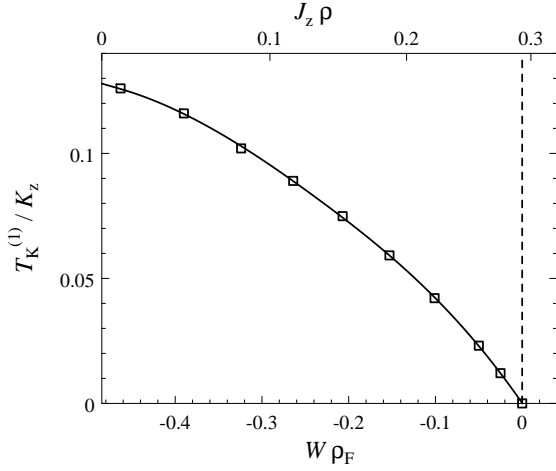


FIG. 9: Phase diagram of the generalized single-impurity Anderson model (14), deduced using the flow equation method. Notation is as in Fig. 7.

follows from the effective hybridization function of the flow equation approach³⁷. The factor $(1 - \Lambda'(0))$ enters in (49) because it generalizes the relation between the Kondo temperature defined in (32) and the renormalized hybridization function within the effective resonant level model³⁷

$$\pi\Delta(0) = \frac{T_K}{w} (1 - \Lambda'(0)) . \quad (51)$$

The results are depicted in Fig. 9. The maximum value of the phase boundary occurring near $J_z = 0$ is given by $(T_K^{(1)}/K_z)_{\max} = 0.126$, which agrees with the extrapolated NRG value 0.11 ± 0.03 from Sect. IV C.

VI. SYMMETRIES AND PERTURBATIONS

To what extent do the results presented in the previous sections depend on the details of the models under consideration? To answer this question we will investigate whether and how (small) perturbations of (3) will qualitatively change the physics. Fermi-liquid phases with vanishing residual entropy S_0 are stable against small perturbations. This is not necessarily the case for our “frozen mini-domain” characterized by $S_0 = \ln 2$. The existence of this $S_0 = \ln 2$ phase is a fundamental feature of our model (3). The necessary conditions for its stability will be discussed in what follows.

Firstly, let us consider the effect of a magnetic field in z -direction acting on the impurity spins. A staggered magnetic field, $h_s(S_1^z - S_2^z)$, will directly destroy the degeneracy of the two configurations $|\uparrow\downarrow\rangle, |\downarrow\uparrow\rangle$. However, in the limit $K_z \rightarrow \infty$ a homogeneous magnetic field $h(S_1^z + S_2^z)$ will not destroy the $S_0 = \ln 2$ phase. It is interesting how these terms modify the generalized Anderson model (14). The magnetic field h results in a term $h \sum_{\sigma} d_{\sigma}^{\dagger} d_{\sigma}$ which breaks particle-hole symmetry in the

generalized Anderson model. It therefore modifies only the position of the phase boundary. The staggered magnetic field h_s , however, will lead to a term $h_s \sum_{\sigma} \sigma d_{\sigma}^{\dagger} d_{\sigma}$ which corresponds to a (pseudo-) magnetic field acting on the pseudospin of the Anderson model. Only the staggered magnetic field is a relevant perturbation which destroys the $\ln 2$ phase.

Apart from these magnetic fields in z -direction there are other relevant terms which lift the twofold degeneracy, which are of the forms:

$$S_j^+ \quad j = 1, 2, \quad (52)$$

$$S_1^+ S_2^-, \quad (53)$$

$$S_1^+ S_2^- \Psi_{i\sigma}^{\dagger} \Psi_{j\sigma} \quad i, j = 1, 2, \quad (54)$$

$$S_1^+ S_2^- \Psi_{i\alpha}^{\dagger} \sigma_{\alpha\beta} \Psi_{j\beta} \quad i, j = 1, 2 \quad (55)$$

and their hermitian conjugates. It turns out that all these operators are forbidden if we impose the following two symmetry conditions: The model should be invariant under the two *separate* spin rotations of each impurity and its electronic bath about an angle of π , i.e., under the transformation

$$U_j = e^{i\pi I_j^z} \quad (56)$$

with $j = 1, 2$. I_j^z is the z -component of spin of system j , $I_j^z = S_j^z + \sum_k c_{k\alpha j}^{\dagger} \frac{1}{2} \sigma_{\alpha\beta}^z c_{k\beta j}$. In the presence of these π rotation symmetries, U_j , the terms (52), (53), (54) and (55) are absent and the frozen mini-domain phase survives. The quantum phase transition from the frozen mini-domain with residual entropy $\ln 2$ to the phase of Kondo screened impurities therefore just relies (in the absence of a staggered magnetic field) on the symmetries U_1 and U_2 .

The model (3) considered in this paper possesses by construction symmetries beyond U_j . They are not necessary for the stability of the $S_0 = \ln 2$ phase. For example, the two baths are assumed to have the same Kondo coupling J_n . This parity symmetry can be relaxed without destroying the frozen mini-domain phase. Furthermore, the z -component of spin of each system, I_j^z , is conserved in our model since we chose $J_x = J_y = J_{\perp}$. This symmetry can also be perturbed without lifting the twofold degeneracy. Moreover, the frozen mini-domain phase is stable against breaking of particle-hole symmetry which we implicitly assumed in the bosonization treatment by linearizing the dispersion relation of the conduction electrons. In all these situations, we therefore expect that all of the *qualitative* results, i.e., the structure of the phase diagram and the nature of the quantum phase transition, are not affected.

However, any perturbation which breaks either U_1 or U_2 (or both) will generically generate one of the relevant couplings (52–55) which all destroy the $\ln 2$ phase. In the following we briefly discuss two such cases which are likely to occur in experimental realizations (a third case, corresponding to (54) is studied in Sec. VII A).

First, consider a situation where a small spin-flip coupling (53) is added on top of the large Ising interaction of the spins,

$$\delta H_{12}^{\perp} = K_{\perp} (S_1^x S_2^x + S_1^y S_2^y). \quad (57)$$

In realizations of our model based on spins and strongly anisotropic spin-orbit interactions, such a term will always be present. A small K_{\perp} will immediately lead to a tunneling between the two states of our mini-domain: their degeneracy is lifted, the two spins form a singlet and the $\ln 2$ residual entropy is quenched completely. Two-impurity Kondo models with $K_{\perp} = K_z$ have been widely studied.^{12,13,14,15,16,17,18,19} As argued in Refs. 16,17 the resulting phase diagram depends on the presence or absence of particle-hole symmetry (which does, however, *not* modify the phase diagram for $K_{\perp} = 0$ as pointed out above). In the absence of particle-hole symmetry, the phase transition is replaced by a smooth crossover. However, in the presence of particle-hole symmetry, the scattering phase shifts of the electrons can only take the values 0 or $\pi/2$. As the Kondo-screened phase and the inter-impurity singlet phase have different phase shifts, there has to be a phase transition in between. This transition is *not* of Kosterlitz-Thouless type, but characterized^{16,18} by a residual entropy $\ln \sqrt{2}$. Nevertheless, this transition will merge with ours in the limit $K_{\perp} \rightarrow 0$, as an infinitesimal K_{\perp} does not affect the Kondo-screened phase but leads immediately to the formation of an inter-impurity singlet in the frozen mini-domain phase.

A second interesting case is a situation where the two Fermi seas are coupled, e.g., by a tunneling between the two leads

$$\delta H_{12}^{\text{tunneling}} = \sum_{k,k',\alpha} \left(t_{kk'} : c_{k\alpha 1}^{\dagger} c_{k'\alpha 2} : + \text{h.c.} \right). \quad (58)$$

While this term is not relevant by power counting, it will induce an RKKY interaction between the spins and therefore generate the relevant coupling (53) or (57). As such a term also breaks particle-hole symmetry, the quantum phase transition will be replaced by a smooth crossover.

VII. TRANSPORT

In this section we illustrate how the phase diagram and, more importantly, the corresponding quantum phase transition can be revealed in transport experiments. We shall discuss two experimental setups: (A) Capacitively coupled quantum dots, where the charge degrees of freedom play the role of (pseudo)spins,^{8,9} are a promising realization of our model. By adding a small inter-dot tunneling term, we obtain a characteristic zero-bias anomaly. (B) If the Ising coupling is realized between real spin degrees of freedom, then we shall show that a transport experiment can reveal a universal fractional critical conductance at the phase transition which

is related to the universal jump of the superfluid density at the Kosterlitz-Thouless transition of superfluid thin films. Using quantum dots this situation is difficult to achieve, as a transverse spin coupling will always be present in the experiment. Nevertheless, the following proposals highlight the non-trivial effects of a Kosterlitz-Thouless transition with a bath of solitonic particles onto the original electrons.

A. Zero-bias anomaly of capacitively coupled quantum dots

In realization of our model (3) using *charge* states of capacitively coupled quantum dots⁸ the conductance discussed above cannot be easily measured. We therefore propose another experiment sketched in Fig. 10. We consider two large quantum dots, each coupled to a (single-channel) lead. The Coulomb interaction and an appropriately chosen gate voltage ensure that two charge states on each dot are degenerate, and that all other charge states have higher energies. These two charge states in each dot take over the role of the two spins as explained in more detail by Matveev.⁸ The spin up and down states of the conduction electrons in our model correspond to electrons sitting either in the leads or on the dot, where we assume that the level spacing on this dot is small compared to temperature. Using this mapping, a capacitive coupling of the two dots directly corresponds to an Ising coupling (1). The physical spin in such a system would translate to an extra channel index in our model. For simplicity we will, however, consider a situation where either strong spin-orbit scattering mixes those channels or where the spin is quenched by a strong magnetic field – in both cases we effectively deal with spinless fermions and thus with a single-channel model.

We now consider a situation where the two dots are coupled by weak tunneling t in addition to the large inter-dot capacity. This tunneling takes the form

$$H_{\text{tun}} = t S_1^+ S_2^- \Psi_{\downarrow 1}^{\dagger}(0) \Psi_{\downarrow 2}(0) + \text{h.c.} \quad (59)$$

We assume that the tunneling is sufficiently weak that it can be treated perturbatively in the experimentally relevant temperature range. This is precisely the situation which was also considered by Andrei *et al.*²⁰ Note that the approximation to consider only tunneling into $\Psi_{\sigma i}(x=0)$ in Eq. (59) is only valid if the tunnel contact between the dots is sufficiently close to the lead contact (see Fig. 10).

We calculate the conductance in perturbation theory in the interdot tunneling t starting from the Kubo formula. The current through the link between the dots is then given by $j = t S_1^+ S_2^- (i \Psi_{\downarrow 1}^{\dagger}(0) \Psi_{\downarrow 2}(0)) + \text{h.c.}$ and the T dependence of the current-current correlator can be obtained from simple power counting.

We first consider the “frozen mini-domain” phase. Following the arguments given in Sec. III, the dimension of the tunneling term (or equivalently of the current

operator) with respect to this fixed point is given by $\dim[H_{\text{tun}}] = \dim[j] = 1 - (\frac{2\delta}{\pi})^2 - (1 - \frac{2\delta}{\pi})^2$. Therefore the current-current correlator decays in time as $t^{-2(\dim[j]-1)}$, and we obtain for the conductance

$$G(T) \sim t^2 T^{-2\dim[j]} = t^2 T^{-4\frac{2\delta}{\pi}(1-\frac{2\delta}{\pi})}. \quad (60)$$

This divergence of the conductance arises because the tunneling is a *relevant* perturbation which will finally destroy the “frozen mini-domain” phase and quench its residual entropy $\ln 2$ below some small energy scale. Eq. (60) is therefore only valid for sufficiently small t when this scale is smaller than T . Furthermore, a finite domain-flip rate induced by (18) is required to obtain a finite current. Above we implicitly assumed that t is so small that the size of the current is solely determined by the smallest bottleneck for charge transport given by t .

At finite voltage $V \gg T$, T in (60) can be replaced by V and we expect a zero-bias anomaly characterized by a pronounced peak in the conductance:

$$G(V) \sim |V|^{-4\frac{2\delta}{\pi}(1-\frac{2\delta}{\pi})}. \quad (61)$$

Upon approaching the quantum phase transition, the divergence increases and at the KT transition takes the universal form

$$G_{cr}(T) \sim T^{-2(\sqrt{2}-1)} \approx T^{-0.83}, \quad (62)$$

$$G_{cr}(V) \sim |V|^{-2(\sqrt{2}-1)} \approx |V|^{-0.83} \quad (63)$$

up to logarithmic corrections.

In the Kondo-screened phase, we can calculate the qualitative behavior of the current-current correlator at the point in the phase diagram where $K_z = 0$ and the dots decouple. The current-current correlator then can be decomposed into two correlators of the form $\langle S_i^+(t) \Psi_{\downarrow i}^\dagger(t) S_i^-(0) \Psi_{\downarrow i}(0) \rangle$ which decay asymptotically as $1/t$. This can be seen if one identifies this correlator with the conduction electron T matrix (see Ref. [40] and references therein) which is characterized by a *constant* spectral density for low energies. The conductance therefore approaches a constant for temperatures and voltages well below the characteristic crossover temperature T^* to the Kondo-screened phase:

$$G(V) \approx G(T) \approx \text{const.} \quad (64)$$

In Fig. 10 we show schematically the nonlinear conductance as a function of V in the vicinity of the quantum phase transition.

In contrast to Eq. (60) and Eq. (64), N. Andrei *et al.*²⁰ obtained an exponentially small conductance in the “frozen mini-domain” phase and $G \sim T^4$ in the singlet phase, with which we disagree.

B. Universal conductance of Ising-coupled quantum dots

What is the most characteristic signature of the Kosterlitz-Thouless quantum phase transition which we

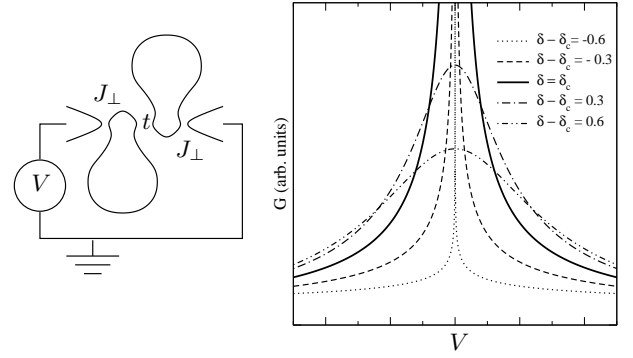


FIG. 10: Left panel: Experimental setup to measure the tunneling conductance between two capacitively coupled quantum dots. Right panel: Schematic plot of the zero bias anomaly of the conductance at $T = 0$. In the “frozen mini-domain” phase, $\delta < \delta_c$, the conductance diverges algebraically according to Eqn. (61). At the quantum phase transition, $\delta = \delta_c$, the exponent takes the universal value $-2(\sqrt{2}-1)$ according to Eq. (62). In the Kondo screened phase, $\delta > \delta_c$, the conductance is finite for $V \rightarrow 0$.

found in the previous sections? The most famous example of a Kosterlitz-Thouless transition is probably the vortex binding-unbinding transition in superfluid ^4He films. From the Kosterlitz-Thouless theory follows the prediction of an universal jump in the superfluid density upon passing through the transition.³⁸

Interestingly, the analogue of the superfluid density in our model is the scattering phase shift δ of the conduction electrons, and the arguments for an universal jump in the superfluid density carry over to an universal jump in δ . This can be seen by considering the RG flow diagram Fig. 3: In the “frozen mini-domain” phase the system flows towards a *line* of fixed points which is naturally characterized by the dimension of the leading irrelevant operator, i.e. the domain flip (18), or, equivalently, according to (21) by the phase shift δ of the conduction electrons. Upon approaching the quantum phase transition, the irrelevant domain flips become marginal and the phase shift increases and reaches $\delta_T = \frac{\pi}{2} \left(1 - \frac{1}{\sqrt{2}}\right)$ at the phase boundary [see Eq. (22)]. On the other side of the phase diagram, the system flows to the strong-coupling fixed *point*, where the Kondo spins are screened and the electrons acquire a phase shift of $\pi/2$. Therefore the phase shift jumps across the transition from δ_T to $\pi/2$! This picture is expected to hold everywhere close to the phase boundary as long as no other phase transition intervenes – that the latter does not happen is shown by our NRG calculations.

This universal jump of the phase shift has direct experimental consequences. Consider the experimental setup sketched in Fig. 11 where the conductance through the left dot is measured. If Kondo screening prevails, the conductance for $T \rightarrow 0$ will be given by the conductance quantum $G_0 = 2e^2/(2\pi\hbar)$. In the frozen mini-domain phase on the other side of the phase diagram, spin flips

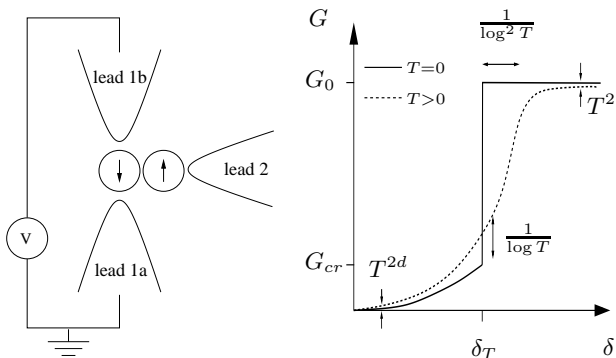


FIG. 11: Left panel: Experimental setup to measure the conductance through a single quantum dot, which is Ising-coupled to a second dot. The couplings to the leads and between the dots can be tuned using appropriate gate voltages. Right panel: At $T = 0$, the conductance (solid line) takes at the quantum phase transition the universal value $G_{cr} = G_0 \cos^2 \frac{\pi}{2\sqrt{2}}$, (66). Dashed line: schematic plot of the conductance at finite T . Corrections to the $T = 0$ result are logarithmic at the transition. The exponent $2d \equiv -2\dim[H_{\text{eff}}^{\text{flip}}]$ is given by the dimension of the domain flip term (18).

are completely suppressed for $T \rightarrow 0$ and therefore we can assume a *static* spin configuration to calculate $G(T = 0)$. For such a potential scattering problem, the conductance is given by

$$G(T = 0) = G_0 \sin^2 \delta. \quad (65)$$

Directly at the quantum phase transition, the conductance therefore takes the universal value

$$G_{cr}(T = 0) = G_0 \sin^2 \delta_T = G_0 \cos^2 \left[\frac{\pi}{2\sqrt{2}} \right] \approx 0.2 G_0, \quad (66)$$

and it jumps to the Kondo value G_0 upon entering the Kondo-screened phase. This universal fractional conductance at our quantum phase transition is one of the remarkable results of this paper.

It is interesting to compare this to the well-known result for the usual Kondo effect, where the conductance jumps from 0 to G_0 when the exchange coupling J is tuned from ferromagnetic to antiferromagnetic. Both in Sec. IIID and Sec. VC we mapped our model close to the quantum phase transition to such a Kondo model. The fermionic degrees of freedom in these Kondo models [Eq. (23) or Eq. (45)] are, however, complex *solitonic* excitations in terms of the original fermions. While the phase shifts of those solitons vanishes at the quantum phase transition, the phase shift of the *physical* electrons takes the fractional value δ_T leading to a fractional conductance. Also in other systems which are described by a Kosterlitz–Thouless quantum transition in terms of solitons, a universal fractional conductance of similar origin can be expected at the transition.

In Fig. 11 the zero-temperature conductance close to the phase transition is shown. At any finite temperatures, the jump in the conductance is strongly smeared as

sketched schematically in the figure. The T -dependence at lowest temperature is determined by the dimension of the leading irrelevant operators. In the Kondo-screened phase leading corrections for $T \rightarrow 0$ to the Kondo conductance G_0 are of order $(T/T^*)^2$ for $T \ll T^*$, where T^* is exponentially small close to the quantum phase transition (see Fig. 6). In the “frozen mini-domain” phase, corrections to (65) vanish as $T^{-2\dim[H_{\text{eff}}^{\text{flip}}]}$ where $\dim[H_{\text{eff}}^{\text{flip}}]$ is defined in Eq. 21. Directly at the quantum phase transition the exponent vanishes and leading corrections to Eq. (66) are of the order $1/\ln T$ and therefore rather large.

VIII. SUMMARY

We have investigated a model of two Ising-coupled Kondo impurities using strong-coupling expansion, numerical renormalization group calculations, and a transformation based on the method of flow equations. Those methods yield consistent results and allowed us to show the existence of a Kosterlitz–Thouless phase transition between a Fermi-liquid phase and a pseudospin doublet phase which corresponds to a “frozen mini-domain”. This transition can be tuned both by varying the Ising coupling between the impurities and by varying the anisotropy of the individual Kondo couplings. In particular, at the Toulouse point of the individual Kondo impurities we could map the model *exactly* to an Anderson impurity model with a Fermi sea consisting of fermionic soliton excitations – in this situation no phase transition occurs, and the system is in the Fermi-liquid phase, where the impurity pseudospin is screened below a collective Kondo scale T^* . For J_z smaller than the Toulouse point value, large K_z drives the system into the pseudospin doublet phase.

The most promising way to realize our model is the situation of capacitively coupled quantum dots where the impurity spins represent charge degrees of freedom on the dots. We have shown that a small additional tunneling between the dots gives rise to a zero-bias conductance anomaly with a *universal* fractional power-law occurring at the transition point. In addition, we have discussed a setup which is interesting on theoretical grounds, namely transport through one quantum dot of a pair of dots with a magnetic Ising coupling, where we have found a *universal* fractional conductance through the device at the phase transition point.

With an eye towards comparison with experiments we discuss the finite-temperature crossover behavior across the phase diagram (see also Fig. 5.) If we fix the parameters of the individual Kondo impurities, then varying K_z corresponds to a vertical cut through the phase diagram in Fig. 1; the resulting finite-temperature behavior is sketched in Fig. 12.

For small K_z there is a single crossover at the single-impurity Kondo temperature $T_K^{(1)}$. This crossover splits

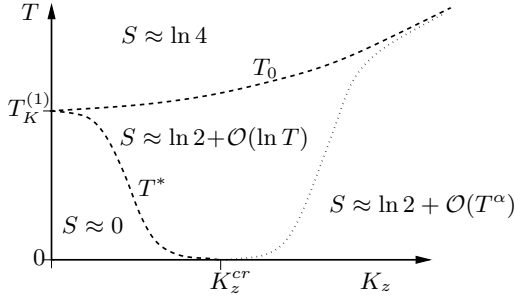


FIG. 12: Schematic phase diagram as a function of K_z and T for fixed $T_K^{(1)}$. For $T = 0$ there is a quantum phase transition at $K_z = K_z^{cr}$ from a Fermi liquid with residual entropy $S_0 = 0$ to the “frozen mini-domain” phase with $S_0 = \ln 2$. At $T > 0$, only smooth crossovers occur indicated by the dashed and dotted lines. At the dashed lines, the entropy S changes by $\ln 2$ (see also Fig. 5), while at the dotted line one obtains a crossover from a logarithmic to a power-law behavior in the leading corrections to S . Similar crossovers also occur in transport quantities. Below T_0 a magnetic “mini-domain” is formed, while a Fermi liquid is recovered below T^* which is exponentially small close to K_z^{cr} .

into two when K_z approaches values of order $T_K^{(1)}$ – then the described two-stage quenching of the entropy is observed. The upper crossover temperature, T_0 , is associated with the formation of the magnetic mini-domain, where relative fluctuations of the two impurity spins are frozen out. The lower crossover temperature is the collective Kondo scale T^* below which the pseudospin of the mini-domain is screened. T^* becomes exponentially small near K_z^{cr} and vanishes for $K_z \geq K_z^{cr}$. For $K_z \geq K_z^{cr}$ another crossover line appears which, however, has much weaker signatures, namely the character of the leading corrections to the entropy and other quantities changes, as is easily understood from the RG flow in Fig. 3. For large K_z the entropy change from $\ln 4$ to $\ln 2$ occurs around $T \sim K_z$, therefore T_0 approaches K_z in this limit.

Interestingly, the different impurity degrees of freedom can be re-interpreted: the flipping of the pseudospin while keeping the mini-domain intact apparently corresponds to pseudospin “phase” fluctuations, whereas breaking up the mini-domain is related to “amplitude” fluctuations of the pseudospin. Thus, in Fig. 12 we encounter the situation that amplitude fluctuations are frozen out at a higher temperature T_0 whereas phase fluctuations are quenched at the lower T^* , in other words, the two impurity spins fluctuate independently for $T > T_0$ whereas they fluctuate in a correlated fashion between $T^* < T < T_0$. This physics is surprisingly similar to the behavior of lattice systems in low dimensions, with the difference that of course no true ordering can occur in the impurity model.

In summary, the present two-impurity model shows remarkably rich behavior, which awaits realizations in mesoscopic devices. An interesting extension would be the two-channel case which is naturally met in capacitively coupled dots with spin-degenerate conduction electrons.

Acknowledgments

The authors acknowledge fruitful discussions with N. Andrei, R. Bulla, L. I. Glazman, K. Le Hur, and A. Schiller. This work has been supported by the Deutsche Forschungsgemeinschaft (DFG) through SFB 484 (SK,TP), the Emmy-Noether program (MG,AR), and the Center for Functional Nanostructures at the University of Karlsruhe (MV). SK also acknowledges support by the DFG through a Heisenberg fellowship.

APPENDIX A: GENERALIZED SCHRIEFER–WOLFF TRANSFORMATION

In this appendix, we perform explicitly the mapping of the generalized Anderson model (14) to the Kondo Hamiltonian (23) for large K_z . Due to the presence of the interaction W in (14) the usual Schrieffer–Wolff transformation has to be generalized to take into account power-law renormalizations (of “x-ray edge” type) induced by W . We derive the mapping by investigating directly the properties of a perturbative expansion in the hybridization V for *finite* W within the Anderson model. Consider the generalized Anderson model in its bosonized version. We first eliminate the W term in (14) by the Emery–Kivelson transformation (9) with $\gamma^* = W\rho$ and obtain

$$U_{\gamma^*} H^A U_{\gamma^*}^\dagger = \sum_{\sigma} H_0[\phi_{\sigma}] + K_z \bar{n}_{d\uparrow} \bar{n}_{d\downarrow} + H_{\text{int}} \quad (\text{A1})$$

where W enters only the hybridization term

$$H_{\text{int}} = \frac{V}{\sqrt{2\pi a}} \sum_{\sigma} \left(d_{\sigma}^\dagger e^{-i(1-W\rho)\phi_{\sigma}(0)} F_{\sigma} + \text{h.c.} \right). \quad (\text{A2})$$

For large K_z the d -level is only singly occupied. V induces virtual fluctuations to the doubly occupied and empty state which are separated from the singly occupied states $|\uparrow\rangle, |\downarrow\rangle$ by an energy $K_z/2$. To derive the effective Kondo model consider the S-matrix with respect to this low-energy subspace:

$$T \exp \left[-i \int_{-\infty}^{\infty} dt H_{\text{int}}(t) \right] = \sum_{n=0}^{\infty} \int_{-\infty}^{\infty} dt_{2n} \dots dt_1 i H_{\text{int}}(t_{2n}) \dots i H_{\text{int}}(t_1) \quad (\text{A3})$$

H_{int} describes processes from the low-energy sector to high energies or back. Such virtual excitations are rare and exist only for a short time if K_z is large. Therefore we can group them to pairs to obtain an effective interaction living in the low-energy Hilbert space,

$$\int_{-\infty}^{t_{2m+1}} dt_{2m} \int_{-\infty}^{t_{2m}} dt_{2m-1} iH_{\text{int}}(t_{2m}) iH_{\text{int}}(t_{2m-1}) \approx -i \int_{-\infty}^{T_{m+1}} H_{\text{int}}^{\text{eff}}(T_m), \quad (\text{A4})$$

with $H_{\text{int}}^{\text{eff}}(T_m) = -i \int_0^\infty dt H_{\text{int}}(T_m + t/2) H_{\text{int}}(T_m - t/2),$

where we introduced the center-of-time and relative coordinates. Interactions between adjacent virtual excitations can be neglected to leading order for large K_z . Introducing the spin notation, $S_z = \frac{1}{2} \sum_\sigma \sigma d_\sigma^\dagger d_\sigma$ and $S^+ = d_\uparrow^\dagger d_\downarrow$, to represent the two states of the low-energy Hilbert space, the above expression becomes

$$H_{\text{int}}^{\text{eff}}(T_m) = -i \frac{V^2}{2\pi a} \int_0^\infty dt e^{-iK_z t/2} \sum_\sigma \left[e^{-i2S_z \sigma(1-W\rho)\phi_\sigma(T_m+t/2)} e^{i2S_z \sigma(1-W\rho)\phi_\sigma(T_m-t/2)} \right. \\ \left. + \left(S^+ F_\uparrow F_\downarrow^\dagger e^{-i\sigma(1-W\rho)\phi_\sigma(T_m+t/2)} e^{i\sigma(1-W\rho)\phi_{-\sigma}(T_m-t/2)} + \text{h.c.} \right) \right].$$

The oscillating factor $e^{-iK_z t/2}$ guarantees that the virtual excitations are only short lived, and we can therefore expand the term in the bracket in the small time t . Introducing the spin field $\phi = \frac{1}{\sqrt{2}} \sum_\sigma \sigma \phi_\sigma$, applying the operator product expansion $e^{i\lambda\phi_\sigma(t)} e^{-i\lambda\phi_\sigma(t')} = (1 + i(t-t')/a)^{-\lambda^2} + \lambda a(1 + i(t-t')/a)^{1-\lambda^2} \partial_{t'} \phi_\sigma(t') + \dots$ for the first term, integrating over t using $\int_0^\infty dt e^{-iK_z t/2} (1 + it/a)^{-\alpha} = -i(aK_z/2)^\alpha 2\Gamma(1-\alpha)/K_z$ we obtain in leading order for large K_z :

$$H_{\text{int}}^{\text{eff}} = \frac{4V^2}{K_z \sqrt{2\pi}} (1-W\rho) \Gamma(2-(1-W\rho)^2) \left(\frac{aK_z}{2} \right)^{(1-W\rho)^2-1} S_z : \partial_x \phi(0) : + \frac{4V^2}{K_z 2\pi a} \left(S^+ e^{-i\sqrt{2}(1-W\rho)\phi(0)} F_\downarrow^\dagger F_\uparrow + \text{h.c.} \right). \quad (\text{A5})$$

Before identifying the coupling constants of the effective low-energy Hamiltonian two more steps are required. First, we have to re-adjust our UV cutoff from a to $a_K \sim 1/K_z$ in the definition of our fields, as we effectively have integrated out short time differences of order $1/K_z$. To this end we have to normal-order $H_{\text{int}}^{\text{eff}}$ as only normal-ordered expressions are cutoff independent,

$$e^{i\lambda\phi} = \left(\frac{2\pi a}{L} \right)^{\frac{\lambda^2}{2}} : e^{i\lambda\phi} : \quad (\text{A6})$$

$$= \left(\frac{a}{a_K} \right)^{\frac{\lambda^2}{2}} \left(\frac{2\pi a_K}{L} \right)^{\frac{\lambda^2}{2}} : e^{i\lambda\phi} : = \left(\frac{a}{a_K} \right)^{\frac{\lambda^2}{2}} e^{i\lambda\tilde{\phi}},$$

where $\tilde{\phi}$ denotes the fields defined with respect to the new cutoff a_K . This effectively leads to the substitution

$$\frac{4V^2}{K_z 2\pi a} \rightarrow \frac{4V^2}{K_z 2\pi a_K} \left(\frac{a}{a_K} \right)^{(1-W\rho)^2-1} \quad (\text{A7})$$

in the second term of (A5).

In a last step, we undo the Emery–Kivelson transformation to obtain the Kondo Hamiltonian in its usual form (23) with

$$J_z^{\text{eff}} = W + \frac{4V^2}{K_z} c_W \left(\frac{aK_z}{2} \right)^{(1-W\rho)^2-1}, \quad (\text{A8})$$

$$J_\perp^{\text{eff}} = \frac{4V^2}{K_z} \left(\frac{a}{a_K} \right)^{(1-W\rho)^2-1}, \quad (\text{A9})$$

where $c_W = (1-W\rho)\Gamma(2-(1-W\rho)^2)$. X-ray edge singularities induced by W have led to a power-law dependence of the effective couplings on K_z . Note that the previous arguments fixed $a_K \sim 1/K_z$ in (A9) only up to a prefactor of order 1 depending on W . However, this unknown prefactor approaches 1 close to the quantum phase transition where $W\rho \rightarrow 0$.

APPENDIX B: FLOW EQUATION TRANSFORMATION FOR THE SINGLE KONDO IMPURITY

In this appendix we provide some details on the flow equation treatment of the single-impurity Kondo model, which was first presented in Ref. 36. Here we will show how to extend the analysis of Ref. 36 to take into account the terms of order $(\lambda^2 - 1)$ that become important in our coupled system since they are multiplied by a possibly large energy scale K_z in (41). We refer the reader to Ref. 36 for the basic ideas of the approach and only present the main steps to keep our presentation here self-contained.

1. Transformation of the Hamiltonian

The starting point for the flow equation approach is (10) with γ chosen such that the longitudinal coupling is eliminated. This way we arrive at the initial Hamiltonian $H(B=0)$ for the flow equation approach

$$H(B) = H_0[\phi] + \int dx g(B; x) (V(\lambda(B); x) S^- + \text{h.c.}) \quad (\text{B1})$$

with $\lambda(B=0) = \lambda_0 = \sqrt{2} - J_z/\sqrt{2}\pi v_F$ and

$$g(B=0; x) = \delta(x) \left(\frac{2\pi a}{L} \right)^{\lambda(B=0)^2/2} \frac{J_\perp}{2\pi a}. \quad (\text{B2})$$

Here $V(\lambda; x)$ are normal ordered vertex operators

$$V(\lambda; x) =: e^{-i\lambda\phi(x)} :. \quad (\text{B3})$$

During the course of the infinitesimal unitary transformations

$$\frac{dH(B)}{dB} = [\eta(B), H(B)] \quad (\text{B4})$$

with the generator $\eta(B)$ from Ref. 36

$$\eta = \int dx \eta^{(1)}(x) (V(\lambda; x) S^- - \text{h.c.}) + \int dx dx' \eta^{(2)}(x, x') [V(\lambda; x), V(-\lambda; x')] \quad (\text{B5})$$

the interaction $g(B; x)$ in (B1) becomes more and more nonlocal. With each infinitesimal step of the transformation one also generates a new interaction term in (B1) with the structure

$$v_F S^z \int dx s(x) \partial_x \phi(x) \quad (\text{B6})$$

and a nonlocal function $s(x)$ that depends on the couplings. The key step in Ref. 36 is that (B6) can again be eliminated by a unitary transformation of the Emery–Kivelson type

$$U =: \exp \left(i S^z \int dx s(x) \phi(x) \right) :. \quad (\text{B7})$$

We now analyze how the interaction term in (B1) is transformed due to U , e.g.

$$U V(\lambda; y) S^- U^\dagger =: \exp \left(-\frac{i}{2} \int dx s(x) \phi(x) \right) : : e^{-i\lambda\phi(y)} : : \exp \left(-\frac{i}{2} \int dx s(x) \phi(x) \right) : S^-. \quad (\text{B8})$$

In order to proceed we normal order all the exponentials, which can be done exactly since the commutator of the bosonic field is a c-number. This leads to

$$U V(\lambda; y) S^- U^\dagger \propto \exp \left(\sqrt{\frac{2\pi}{L}} \sum_{k>0} \frac{e^{-ka/2}}{\sqrt{k}} ([\lambda e^{-iky} + s(k)] b_k - [\lambda e^{iky} + s(k)] b_k^\dagger) \right) : S^- \quad (\text{B9})$$

with $s(k)$ being the Fourier transform of $s(x)$ from (B6). The proportionality factor in (B9) leads to the non-perturbative renormalization of the coupling constant $g(B; x)$ already obtained in Ref. 36. Except for the local coupling at the beginning of the flow the exponential in (B9) cannot be exactly rewritten as a vertex operator. We use two approximations that give us the correct result up to quadratic terms in the deviation from the Toulouse line: i) We use the infrared limit $s(0)$ instead of $s(k)$ in (B9). ii) We expand the exponential in a way that avoids IR-divergences and neglect higher order terms in the bosonic operators that lead to irrelevant couplings:

$$\begin{aligned} & : \exp \left(\sqrt{\frac{2\pi}{L}} \sum_{k>0} \frac{e^{-ka/2}}{\sqrt{k}} ([\lambda e^{-iky} + s(0)] b_k - \text{h.c.}) \right) : \\ &= : \exp \left(\sqrt{\frac{2\pi}{L}} \sum_{k>0} \frac{e^{-ka/2}}{\sqrt{k}} ((\lambda + s(0)) e^{-iky} + (1 - e^{-iky}) s(0)) b_k - \text{h.c.} \right) : \\ &= : V(\lambda + s(0); y) \left(1 + \sqrt{\frac{2\pi}{L}} \sum_{k>0} \frac{e^{-ka/2}}{\sqrt{k}} ((1 - e^{-iky}) s(0) b_k - \text{h.c.}) + \dots \right) :. \end{aligned} \quad (\text{B10})$$

Retaining only the first term on the right-hand side is the approximation used in Ref. 36: one obtains vertex operators with flowing scaling dimensions $[\lambda + s(0)]$ that

eventually become fermionic. The second term can be understood as a correction term to this leading behavior due to the nonlocality of the interaction during the flow

equation procedure. It is this term that eventually leads to the correction term in (42).

The above procedure following from (B8) has to be repeated iteratively throughout the flow, leading to

$$\begin{aligned}
& : V(1; y) \left(1 + (1 - \lambda_0) \sqrt{\frac{2\pi}{L}} \sum_{k>0} \frac{e^{-ka_{TK}/2}}{\sqrt{k}} \right. \\
& \quad \left. \times ((1 - e^{-iky}) b_k - \text{h.c.}) \right) : S^- \\
& = : \Psi^\dagger(y) \left(1 + (1 - \lambda_0) (-i\bar{\phi}(0) + i\bar{\phi}(y)) \right) : S^- \\
& = : \Psi^\dagger(y) \left(1 + (1 - \lambda_0) iy \partial_y \bar{\phi}(0) \right) : S^- \quad (\text{B11})
\end{aligned}$$

plus irrelevant terms with higher order derivatives of the bosonic field. Here $\bar{\phi}(y)$ denotes the bosonic spin-density field $\phi(y)$ without the Fourier components for energies larger than $\mathcal{O}(T_K)$ since the term proportional to $(1 - \lambda_0)$ is generated successively during the flow equation procedure. Putting everything together, the Hamiltonian $H(B)$ from (B1) acquires a new term of order $(1 - \lambda_0)$ during the flow that has been neglected in Ref. 36. It can be viewed as an assisted hopping term that is marginal as opposed to the leading order hopping term that is a relevant operator. The new term can be eliminated by including an additional term with the structure

$$\int dx \eta^{(3)}(x) \left(: V(\lambda; x) \partial_x \bar{\phi}(0) : S^- - \text{h.c.} \right) \quad (\text{B12})$$

and a suitable coefficient function $\eta^{(3)}(x)$ into the generator (B6). One can verify that this does not modify the

previous flow equations for the Hamiltonian in linear order in $\eta^{(3)}(x)$ (essentially since the assisted hopping term is marginal as opposed to the relevant hopping term that generates the flow equations in leading order). Therefore we can neglect these extra terms in the flow of the Hamiltonian when we want to retain terms up to linear order in $(\lambda_0 - 1)$.

2. Transformation of the impurity spin operator

However, for the transformation of S^z one needs to be more careful since S^z can be multiplied by a large exchange field $h = \pm K_z/2$ due to the coupling to the second spin. This can be much larger than the Kondo scale close to the transition. In order to study the transformation of S^z we follow the same route as in Ref. 36 by using the identity $S^z = [S^+, S^-]/2$ and evaluating the transformed \tilde{S}^+ (\tilde{S}^- then follows as its hermitean conjugate). One needs to study the additional effect of (B12) on S^+ and finds the following expression in the low-energy limit:

$$\tilde{S}^+ = \sigma_z \int dy d(y) : \Psi^\dagger(y) (1 + (1 - \lambda_0) iy \partial_y \bar{\phi}(0)) : \quad (\text{B13})$$

with [to linear order in $(\lambda_0 - 1)$] the same coefficients $d(y)$ as in Ref. 36. This leads to

$$\begin{aligned}
\tilde{S}^z &= [\tilde{S}^+, \tilde{S}^-]/2 = \frac{1}{2} \int dx dx' d(x) d^*(x') [\Psi^\dagger(x), \Psi(x')] + \frac{1}{2} (1 - \lambda_0) \int dx dx' d(x) d^*(x') \\
&\quad \times (-ix' [\Psi^\dagger(x), : \Psi(x') \partial_{x'} \bar{\phi}(0) :] + ix [: \Psi^\dagger(x) \partial_x \bar{\phi}(0) :, \Psi(x')]) + \mathcal{O}((\lambda_0 - 1)^2). \quad (\text{B14})
\end{aligned}$$

Since we are interested in an analysis in the vicinity of the Toulouse line we only keep terms up to linear order in $(\lambda_0 - 1)$. The term of order $(\lambda_0 - 1)$ consists of two fermionic operators and a spatial derivative of the bosonic field. If we subtract the contractions with respect to the ground state the remaining normal ordered operator will therefore lead to an irrelevant coupling in the coupled Hamiltonians (39). However, we need to retain the contractions:

$$\begin{aligned}
\tilde{S}^z &= \frac{1}{2} \int dx dx' d(x) d^*(x') [\Psi^\dagger(x), \Psi(x')] + \frac{1}{2} (1 - \lambda_0) iy \partial_x \bar{\phi}(0) \int dx dx' d(x) d^*(x') (x - x') \langle [\Psi^\dagger(x), \Psi(x')] \rangle \\
&\quad + \mathcal{O}((\lambda_0 - 1)^2) + \text{irrelevant} \\
&= \frac{1}{2} \int dx dx' d(x) d^*(x') [\Psi^\dagger(x), \Psi(x')] + \frac{1}{2} (\lambda_0 - 1) f(h) \partial_x \bar{\phi}(0) + \mathcal{O}((\lambda_0 - 1)^2) + \text{irrelevant} \quad (\text{B15})
\end{aligned}$$

with

$$f(h) \stackrel{\text{def}}{=} \int dk dk' (\partial_k d_k d_{k'} + d_k \partial_{k'} d_{k'}) \langle [\Psi_k^\dagger, \Psi_{k'}] \rangle. \quad (\text{B16})$$

Here d_k denotes the Fourier transform of $d(x)$. The expectation value $\langle [\Psi_k^\dagger, \Psi_{k'}] \rangle$ has to be evaluated in the ground state of the Hamiltonian $H^{(\text{pot})}$ that is obtained from the resonant level model Hamiltonian plus magnetic field $h S^z$

after the above unitary transformation. Since S^z “decays” into fermion operators under this transformation according to (B14), this Hamiltonian is given as

$$H^{(\text{pot})} = \sum_k \epsilon_k \Psi_k^\dagger \Psi_k + \sum_{k,k'} h d_k d_{k'} \Psi_k^\dagger \Psi_{k'}, \quad (\text{B17})$$

i.e. this is just a potential scattering model with a separable potential $V_{kk'} = h d_k d_{k'}$. The retarded Green’s function can be calculated in closed form

$$G_{kk'}(\epsilon^+) = \frac{\delta_{kk'}}{\epsilon^+ - \epsilon_k} + \frac{h d_k d_{k'}}{(\epsilon^+ - \epsilon_k)(\epsilon^+ - \epsilon_{k'})} \frac{1}{1 - \sum_q \frac{h d_q^2}{\epsilon^+ - \epsilon_q}} \quad (\text{B18})$$

leading to

$$\begin{aligned} f(h) &= \int dk dk' (\partial_k d_k d_{k'} + d_k \partial_{k'} d_{k'}) \langle [\Psi_k^\dagger, \Psi_{k'}] \rangle \\ &= -\frac{1}{\pi} \text{Im} \int dk dk' (\partial_k d_k d_{k'} + d_k \partial_{k'} d_{k'}) \left(\int_{-\infty}^0 d\epsilon G_{kk'}(\epsilon^+) - \int_0^\infty d\epsilon G_{kk'}(\epsilon^+) \right) \\ &= -\frac{1}{\pi} \text{Im} \left(\int_{-\infty}^0 d\epsilon - \int_0^\infty d\epsilon \right) \int dk \frac{\partial_k d_k^2}{\epsilon^+ - \epsilon_k} \\ &\quad - h \frac{1}{\pi} \text{Im} \left(\int_{-\infty}^0 d\epsilon - \int_0^\infty d\epsilon \right) \int dk \frac{\partial_k d_k^2}{\epsilon^+ - \epsilon_k} \int dk' \frac{d_{k'}^2}{\epsilon^+ - \epsilon_{k'}} \frac{1}{1 - \sum_q \frac{h d_q^2}{\epsilon^+ - \epsilon_q}}. \end{aligned} \quad (\text{B19})$$

One easily shows that the impurity orbital Green’s function $G_{dd}^{(\epsilon_d=0)}(\epsilon^+)$ in the resonant level model

$$H^{(RLM)} = \sum_k \epsilon_k \Psi_k^\dagger \Psi_k + \sum_k \tilde{V} (d^\dagger \Psi_k + \Psi_k^\dagger d) \quad (\text{B20})$$

is given by

$$G_{dd}^{(\epsilon_d=0)}(\epsilon^+) = \sum_q \frac{d_q^2}{\epsilon^+ - \epsilon_q}. \quad (\text{B21})$$

Using

$$\sum_q \frac{\partial_q d_q^2}{\epsilon^+ - \epsilon_q} = v_F \partial_\epsilon G_{dd}^{(\epsilon_d=0)}(\epsilon^+) \quad (\text{B22})$$

one can reexpress (B19) as

$$\begin{aligned} f(h) &= 2v_F \rho_d^{(\epsilon_d=0)}(0) \\ &\quad - v_F h \frac{1}{\pi} \text{Im} \left(\int_{-\infty}^0 d\epsilon - \int_0^\infty d\epsilon \right) \left(\partial_\epsilon G_{dd}^{(\epsilon_d=0)}(\epsilon^+) \right) \\ &\quad \times G_{dd}^{(\epsilon_d=0)}(\epsilon^+) \frac{1}{1 - h G_{dd}^{(\epsilon_d=0)}(\epsilon^+)}, \end{aligned} \quad (\text{B23})$$

where $\rho_d^{(\epsilon_d=0)}(\epsilon)$ is the impurity orbital density of states. One notices that the impurity orbital Green’s function in the resonant level model with nonvanishing impurity orbital energy $\epsilon_d d^\dagger d$ can be written as

$$G_{dd}^{(\epsilon_d)}(\epsilon^+) = \frac{G_{dd}^{(\epsilon_d=0)}(\epsilon^+)}{1 - \epsilon_d G_{dd}^{(\epsilon_d=0)}(\epsilon^+)} \quad (\text{B24})$$

which leads to

$$\begin{aligned} f(h) &= 2v_F \rho_d^{(\epsilon_d=0)}(0) \\ &\quad - v_F h \frac{1}{\pi} \text{Im} \left(\int_{-\infty}^0 d\epsilon - \int_0^\infty d\epsilon \right) \\ &\quad \times \left(\partial_\epsilon G_{dd}^{(\epsilon_d=0)}(\epsilon^+) \right) G_{dd}^{(\epsilon_d=h)}(\epsilon^+). \end{aligned} \quad (\text{B25})$$

This expression can be easily worked out in various limits

$$f(h) = \begin{cases} 2w v_F / T_K^{(1)} & \text{for } h = 0 \\ v_F / |h| & \text{for } |h| \gg T_K^{(1)} \end{cases} \quad (\text{B26})$$

and a smooth crossover in between (here $w = 0.4128$ is the Wilson number).

¹ A. C. Hewson, *The Kondo Problem to Heavy Fermions*, Cambridge University Press, Cambridge (1997).

² K. G. Wilson, Rev. Mod. Phys. **47**, 773 (1975).

³ N. Andrei, K. Furuya, and J. H. Lowenstein, Rev. Mod.

Phys. **55**, 331 (1983); A. M. Tsvelick and P. B. Wiegmann, Adv. Phys. **32**, 453 (1983).

⁴ S. Doniach, Physica B **91**, 231 (1977).

⁵ A. H. Castro-Neto and B. A. Jones, Phys. Rev. B **62**, 14975

- (2000).
- ⁶ A. J. Millis, D. K. Morr, and J. Schmalian, Phys. Rev. Lett. **87**, 167202 (2001), Phys. Rev. B **66**, 174433 (2002).
 - ⁷ F. R. Waugh, M. J. Berry, D. J. Mar, R. M. Westervelt, K. L. Campman, and A. C. Gossard, Phys. Rev. Lett. **75**, 705 (1995).
 - ⁸ K. A. Matveev, Zh. Eksp. Teor. Fiz. **99**, 1598 (1991) [Sov. Phys. JETP **72**, 892 (1991)].
 - ⁹ K. A. Matveev, L. I. Glazman, and H. U. Baranger, Phys. Rev. B **53**, 1034 (1996).
 - ¹⁰ J. M. Golden and B. I. Halperin, Phys. Rev. B **53**, 3893 (1996).
 - ¹¹ J. E. Mooij, T. P. Orlando, L. Levitov, L. Tian, C. H. van der Wal, and S. Lloyd, Science **285**, 1036 (1999).
 - ¹² C. Jayaprakash, H. R. Krishnamurthy, and J. W. Wilkins, Phys. Rev. Lett. **47**, 737 (1981).
 - ¹³ B. A. Jones, C. M. Varma, and J. W. Wilkins, Phys. Rev. Lett. **61**, 125 (1988); B. A. Jones and C. M. Varma, Phys. Rev. B **40**, 324 (1989).
 - ¹⁴ O. Sakai, Y. Shimizu, and T. Kasuya, Solid State Comm. **75**, 81 (1990); O. Sakai and Y. Shimizu, J. Phys. Soc. Jpn **61**, 2333 (1992), *ibid*, **61**, 2348 (1992).
 - ¹⁵ R. M Fye, Phys. Rev. Lett. **72**, 916 (1994).
 - ¹⁶ I. Affleck, A. W. W. Ludwig, and B. A. Jones, Phys. Rev. B **52**, 9528 (1995).
 - ¹⁷ A. J. Millis, B. G. Kotliar, and B. A. Jones, in *Field Theories in Condensed Matter Physics*, edited by Z. Tesanovic (Addison-Wesley, Redwood City, CA, 1990), pp. 159-166.
 - ¹⁸ J. Gan, Phys. Rev. Lett. **74**, 2583 (1995); **74**, 5287 (1995); Phys. Rev. B **51**, 8287 (1995).
 - ¹⁹ J. B. Silva, W. L. C. Lima, W. C. Oliveira, J. L. N. Mello, L. N. Oliveira, and J. W. Wilkins, Phys. Rev. Lett. **76**, 275 (1996).
 - ²⁰ N. Andrei, G. T. Zimanyi, and G. Schön, Phys. Rev. B **60**, R5125 (1999).
 - ²¹ G. D. Mahan, *Many-Particle Physics*, Kluwer Academic, Amsterdam (2000).
 - ²² U. Weiss, *Quantum Dissipative Systems* (World Scientific, Singapore, 1999).
 - ²³ A. J. Leggett, S. Chakravarty, A. T. Dorsey, M. P. A. Fisher, A. Garg, and W. Zwerger, Rev. Mod. Phys. **59**, 1 (1987).
 - ²⁴ K. Kassner, J. Phys. B (Cond. Matt.) **81**, 245 (1990).
 - ²⁵ M. J. Storcz and F. K. Wilhelm, Phys. Rev. A **67**, 042319 (2003).
 - ²⁶ P. Schlottman, J. Phys. (Paris) **6**, 1486 (1978).
 - ²⁷ For an overview of refermionization see J. von Delft and H. Schoeller, Ann. Physik (Leipzig) **7**, 225 (1998). Notice that different fermion species do not anticommute, which, however, does not affect the equations of motion.
 - ²⁸ G. Toulouse, C. R. Acad. Sci. Paris **268**, 1200 (1969).
 - ²⁹ G. Yuval and P. W. Anderson, Phys. Rev. B **1**, 1522 (1970); P. W. Anderson, G. Yuval, and D. R. Hamann, Phys. Rev. B **1**, 4464 (1970).
 - ³⁰ P. W. Anderson, Phys. Rev. Lett. **18**, 1049 (1967), Phys. Rev. **164**, 352 (1967).
 - ³¹ J. J. Hopfield, Comments Solid State Phys. **2**, 40 (1969).
 - ³² K. D. Schotte and U. Schotte, Phys. Rev. **182**, 479 (1969).
 - ³³ A. O. Gogolin, A. A. Nersisyan, and A. M. Tsvelik, *Bosonization and Strongly Correlated Systems*, Cambridge University Press, Cambridge (1998).
 - ³⁴ J. M. Kosterlitz, J. Phys. C **7**, 1046 (1974).
 - ³⁵ F. Wegner, Ann. Physik (Leipzig) **3**, 77 (1994).
 - ³⁶ W. Hofstetter and S. Kehrein, Phys. Rev. B **63**, 140402(R) (2001).
 - ³⁷ C. Slezak, S. Kehrein, Th. Pruschke, and M. Jarrell, Phys. Rev. B **67**, 184408 (2003).
 - ³⁸ D. R. Nelson and J. M. Kosterlitz, Phys. Rev. Lett. **39**, 1201 (1977).
 - ³⁹ A preliminary account on the flow-equation analysis of the present model appeared in S. Kehrein and M. Vojta, cond-mat/0208390. The initial version of this preprint did not consider the corrections described in Sec. V B arising from the deviations from the Toulouse point, and incorrectly concluded that no phase transition occurs even away from the Toulouse point.
 - ⁴⁰ A. Rosch, T. A. Costi, J. Paaske, and P. Wölfle, cond-mat/0301106.